Journal of Clinical Microbiology

Characterization of Enterohemorrhagic Escherichia coli O111 and O157 Strains Isolated from Outbreak Patients in Japan

Masanori Watahiki, Junko Isobe, Keiko Kimata, Tomoko Shima, Jun-ichi Kanatani, Miwako Shimizu, Akihiro Nagata, Keiko Kawakami, Mikiko Yamada, Hidemasa Izumiya, Sunao Iyoda, Tomoko Morita-Ishihara, Jiro Mitobe, Jun Terajima, Makoto Ohnishi and Tetsutaro Sata

J. Clin. Microbiol. **2014, 52(8):2757. DOI: 10.1128/JCM.00420-14.**
Published Ahead of Print 14 May 2014.

JCM
Journals.ASM.org

Characterization of Enterohemorrhagic *Escherichia coli* O111 and O157 Strains Isolated from Outbreak Patients in Japan

Masanori Watahiki,[a] Junko Isobe,[a] Keiko Kimata,[a] Tomoko Shima,[a] Jun-ichi Kanatani,[a] Miwako Shimizu,[a] Akihiro Nagata,[b]* Keiko Kawakami,[c] Mikiko Yamada,[d] Hidemasa Izumiya,[e] Sunao Iyoda,[e] Tomoko Morita-Ishihara,[e] Jiro Mitobe,[e] Jun Terajima,[e]* Makoto Ohnishi,[e] Tetsutaro Sata[a]

Toyama Institute of Health, Toyama, Japan[a]; Fukui Prefectural Institute of Public Health and Environment Science, Fukui, Japan[b]; Ishikawa Prefectural Institute of Public Health and Environmental Science, Ishikawa, Japan[c]; Yokohama City Institute of Health, Kanagawa, Japan[d]; National Institute of Infectious Diseases, Tokyo, Japan[e]

In April and May 2011, there was a serious food-poisoning outbreak in Japan caused by enterohemorrhagic *Escherichia coli* (EHEC) strains O111:H8 and O157:H7 from raw beef dishes at branches of a barbecue restaurant. This outbreak involved 181 infected patients, including 34 hemolytic-uremic syndrome (HUS) cases (19%). Among the 34 HUS patients, 21 developed acute encephalopathy (AE) and 5 died. Patient stool specimens yielded *E. coli* O111 and O157 strains. We also detected both EHEC O111 stx_2 and *stx*-negative *E. coli* O111 strains in a stock of meat block from the restaurant. Pulsed-field gel electrophoresis (PFGE) and multilocus variable-number tandem-repeat analysis (MLVA) showed that the *stx*-negative *E. coli* O111 isolates were closely related to EHEC O111 stx_2 isolates. Although the EHEC O157 strains had diverse *stx* gene profiles (stx_1, stx_2, and stx_1 stx_2), the PFGE and MLVA analyses indicated that these isolates originated from a single clone. Deletion of the Stx2-converting prophage from the EHEC O111 stx_2 isolates was frequently observed during *in vitro* growth, suggesting that strain conversion from an EHEC O111 stx_2 to an *stx*-negative strain may have occurred during infection.

Enterohemorrhagic *Escherichia coli* (EHEC) strains cause a variety of human illnesses, such as uncomplicated diarrhea, hemorrhagic colitis, hemolytic-uremic syndrome (HUS), and related acute encephalopathy (1). Shiga toxin 1 (Stx1) and Stx2 are EHEC virulence factors that cause endothelial cell damage with consecutive systemic thrombotic microangiopathy, resulting in hemorrhagic colitis and subsequent renal failure and involvement of other organs (1–4).

EHEC infection is a category III notifiable infectious disease in Japan, according to the Law Concerning the Prevention of Infectious Diseases and Medical Care for Patients of Infections (Infectious Diseases Control Law). All EHEC cases must be reported by the physician who made the diagnosis. Prefectural and municipal public health institutes (PHIs) conduct EHEC isolation, serotyping, and verotoxin (VT) typing and report their results to the Infectious Disease Surveillance Center (IDSC) of the National Institute of Infectious Diseases (NIID), Japan. Approximately 4,000 cases are reported annually. O157 is the most common EHEC serogroup in gastrointestinal tract infections, accounting for 60 to 70% of the reported EHEC infections. Among non-O157 EHEC serogroups, O26 is the second most common serogroup, accounting for 20 to 25% of the EHEC cases, followed by serogroups O111, O121, and O103.

Hemolytic-uremic syndrome (HUS) is an illness characterized by acute kidney injury, thrombocytopenia, and microangiopathic hemolytic anemia. Approximately 100 HUS cases associated with EHEC infections are reported annually in Japan, corresponding to 3 to 4% of the symptomatic EHEC infections. EHEC O157 is the most prevalent EHEC serogroup causing HUS, accounting for approximately 90% of the HUS cases identified among EHEC isolates. However, a wide variety of EHEC non-O157 serogroups might also cause HUS.

The EHEC O111 serogroup is the etiological agent of approximately 4% of the EHEC cases in Japan (5). During 2006 to 2010, there were 83 EHEC outbreaks in Japan, in which 10 or more EHEC-positive cases were reported. Six of these outbreaks were caused by EHEC O111 strains (6–10): three by EHEC O111 stx_1 strains, and the other three by EHEC O111 stx_1 stx_2 strains. EHEC O111 stx_2 isolates are very rare in Japan, consistent with data from other countries (11–13). Although some serious outbreaks due to EHEC O111 isolates have been reported in Western countries (14–16), EHEC O111 outbreaks with serious complications, like HUS, have been rare in Japan.

The important EHEC virulence factors are Stx1 and Stx2 and the locus of enterocyte effacement (LEE) element that is responsible for intimate adhesion to host intestinal cells. The stx_1 and stx_2 genes are encoded in different but similar prophage genomes. The loss and gain of these prophages must affect EHEC virulence. Since Stx-converting phages have been reported to be lost during *in vitro* culture (17, 18), they may also be lost under *in vivo* conditions, although no conclusive *in vivo* data are currently available.

There was a large EHEC outbreak in Japan in April and May 2011. A case-control study showed that raw beef dishes consumed at a chain of barbecue restaurants were the vehicles for these infections (Y. Yahata, T. Misaki, Y. Ishida, M. Nagira, M. Watahiki, J. Isobe, J. Terajima, S. Iyoda, J. Mitobe, M. Ohnishi, T. Sata, K.

Received 14 February 2014 Returned for modification 18 March 2014
Accepted 10 May 2014
Published ahead of print 14 May 2014
Editor: D. J. Diekema
Address correspondence to Masanori Watahiki, masanori.watahiki@pref.toyama.lg.jp.
* Present address: Akihiro Nagata, Fukui Health and Welfare Center, Fukui, Japan; Jun Terajima, National Institute of Health Science, Tokyo, Japan.

doi:10.1128/JCM.00420-14

Taniguchi, Y. Tada, N. Okabe, and *E. coli* Outbreak Investigation Team, unpublished data). A total of 941 individuals ate at the restaurant chain from 19 April to 4 May 2011, and 181 presented as outbreak-related cases, including 34 HUS cases. Only 55 of the 181 infections were confirmed by laboratory isolation to be from the EHEC O111 and/or O157 serogroups. Of the 34 HUS cases, 21 developed acute encephalopathy and 5 died. Here, we report studies characterizing the *E. coli* O111 and O157 strains isolated from the cases in this outbreak.

MATERIALS AND METHODS

Case definition. The case definition for the 181 patients in this outbreak was a person who developed illness >10 h after eating at one of the restaurants in the implicated restaurant chain in April 2011, and who presented with at least one of the following symptoms: (i) bloody stools, (ii) more than two gastrointestinal symptoms, such as diarrhea, nausea or vomiting, abdominal pain, and tenesmus, (iii) one of the gastrointestinal symptoms in addition to at least two additional symptoms, such as fever (temperature of >37.5°C), malaise, or headache, or (iv) a stool culture positive for *E. coli* O111, EHEC O111, or EHEC O157.

Strains. A total of 104 EHEC O111, EHEC O157, and *stx*-negative *E. coli* O111 isolates were collected from three public health centers in Toyama Prefecture, Japan, and sent to the Toyama Institute of Health (TIH). EHEC strains were also obtained from public health institutes in Fukui Prefecture, Ishikawa Prefecture, Kanazawa City, and Yokohama City, where related cases were detected. EHEC O111 strain 11128 (19) and EHEC O157 strain Sakai (20), used as reference strains, were obtained from the National Institute of Infectious Diseases (Tokyo, Japan) and the Research Institute for Microbial Diseases, Osaka University (Osaka, Japan), respectively.

Isolation of EHEC and serotyping. Specimens were collected from seven public health and medical laboratories (listed in Acknowledgments). Stool specimens (n = 188) from patients, samples from leftover food from the implicated restaurants (n = 20), and smear samples from the implicated restaurant kitchens (n = 14) were collected and sent to the TIH for analysis. For EHEC isolation, the specimens were analyzed by enrichment culture, immunomagnetic separation (IMS) (21) with O111 or O157 lipopolysaccharide (LPS) antibodies, and acid treatment before plating on selective agar medium, as described below (22). The enriched samples were spread on cefixime-tellurite (CT)-MacConkey sorbitol agar, CT-MacConkey sorbose agar, CHROMagar O157 TAM, CT-CHROMagar O157 TAM, or CHROMagar Shiga toxigenic *E. coli* (STEC). After the plates were incubated overnight at 35°C, the isolated colonies were transferred to Trypticase soy agar (TSA) plates (Becton, Dickinson and Company), and these plates were incubated at 35°C overnight. The colonies (>4) isolated from the TSA plates were tested by PCR for the presence of the stx_2 gene and serotyped using anti-*E. coli* O111 and O157 antisera (Denka Seiken Co., Ltd., Tokyo, Japan). Determination of the flagellar antigen type of the EHEC O111 outbreak strain was carried out by *fliC* typing with PCR-restriction fragment length polymorphism (23). The PCR amplicons were digested with HhaI (Nippon Gene Co., Ltd., Toyama, Japan) and separated by 2% agarose gel electrophoresis.

Pulsed-field gel electrophoresis. Pulsed-field gel electrophoresis (PFGE) was performed using the PulseNet protocol (24). Genomic DNA in agarose plugs was digested overnight with 30 U XbaI (Nippon Gene Co. Ltd., Toyama, Japan) at 37°C. Electrophoresis of the XbaI-treated plugs was performed with the CHEF Mapper system (Bio-Rad Laboratories) using pulsed-field certified agarose (Bio-Rad Laboratories) with 0.5× Tris-borate-EDTA (TBE) running buffer. The electrophoretic conditions were as follows: 6 V/cm for 19 h, pulse time ranging from 2.2 to 54.2 s, and 0.5× TBE buffer at 12°C. *Salmonella enterica* subsp. *enterica* serovar Braenderup genomic DNA in an agarose plug was also digested overnight with 30 U XbaI and used as a molecular size marker. After electrophoresis, the gels were stained with ethidium bromide (final concentration, 50 ng/ml), destained by washing with distilled water, and photographed with ChemiDoc XRS (Bio-Rad Laboratories).

Multilocus variable-number tandem-repeat analysis. Multilocus variable-number tandem-repeat analysis (MLVA) was carried out as described in previous reports (25, 26). The PCR products labeled at the 5′ termini of the target loci for MLVA were separated using an ABI 3130xl Genetic Analyzer (Applied Biosystems). The repeat copy number for a null allele (i.e., when no PCR product was obtained) was designated −2.

Detection of virulence-related genes. Test strains were selected from 10, nine, five, two, and two representative isolates of the EHEC O111:H8 stx_2, *stx*-negative *E. coli* O111, EHEC O157 stx_1 stx_2, EHEC O157 stx_1, and EHEC O157 stx_2 isolates, respectively. The *E. coli* strains were resuspended in 200 μl of 5% (wt/vol) Chelex 100 resin (27) and heated for 10 min at 100°C. After centrifugation, the supernatants were quantified by using a NanoDrop ND-1000 (Thermo Fisher Scientific). The DNA preparations were diluted to a final concentration of 10 ng/μl and used as a template for PCR. The PCR primers used to detect *stx* genes were commercially purchased EVC-1 and EVC-2 to simultaneously detect common *stx* genes, EVT-1 and EVT-2 to detect stx_1, and EVS-1 and EVS-2 to detect stx_2 (TaKaRa Bio, Inc.). Other virulence-related genes were analyzed by a multiplex PCR-based protocol (28). The target genes were stx_1, stx_2, *eae*, CVD432, *aggR*, *invE*, *elt* (labile toxin [LT] gene), *esth* (saitohin [STh] gene), *estp* (sulfotransferase [STp] gene), *bfp*, EAF, and *astA*. The Stx-encoding genes, stx_1 and stx_2, of the EHEC isolates in this outbreak were subtyped using PCR (29).

To detect the *norV* gene (30), a primer pair was designed from the EHEC O111 genome *norV* sequence (GenBank accession no. AP010960): norV-337f (5′-CAT ACC TCA CCG AGT G-3′) and norV-914r (5′-GAG CGG AAG ACA TTG GTC AGG-3′). To detect the *ospG* gene (31), the primer pair was ospG-F (5′-CCA TTT GAG AAT AAT AAT TCT CAT GCT G-3′) and ospG-R (5′-GCA TTT GTA ATC GTC GGT CGA TAA TC-3′).

Titration of Stx in EHEC cultures. To detect Shiga toxin in the culture medium of the EHEC isolates, the strains were grown in Casamino Acid-yeast extract (CA-YE) medium (Denka Seiken Co., Ltd., Tokyo, Japan) overnight with shaking at 35°C. Each culture was centrifuged (900 × *g* for 15 min), and the supernatant was used for the Stx1 and Stx2 assays. Each toxin was detected in a 2-fold dilution series of the supernatant by a verotoxin *E. coli* reversed passive latex agglutination assay (VTEC-RPLA) (Denka Seiken Co., Ltd., Tokyo, Japan), according to the manufacturer's specifications. The toxin titers were expressed as the maximum dilution with a positive reaction.

RESULTS

Isolation of EHEC from patients. During this outbreak, we identified 34 patients with HUS cases and, in the early phase of the outbreak, *stx*-negative *E. coli* O111-positive cases were identified. Therefore, we reexamined the stool specimens that had given culture-negative results. After enrichment using anti-LPS (O111 or O157) antibody-conjugated magnetic beads, multiple colonies (usually 4 or more; at most, 800 colonies) were checked for *stx* genes. A total of 55 patients were found to be positive for EHEC O111 with $fliC_{H8}$ and/or O157 with $fliC_{H7}$. These laboratory-confirmed cases were divided into three groups: only EHEC O111 isolated (group 1), both EHEC O157 and O111 isolated (group 2), and only EHEC O157 isolated (group 3). The groups contained 25, 12, and 18 cases, respectively (Table 1). Of the 37 EHEC O111-positive cases (groups 1 and 2), 17 developed HUS, including 13 cases of acute encephalopathy. However, of the 30 EHEC O157-positive cases (groups 2 and 3), only 9 cases developed HUS, including 6 cases of acute encephalopathy. Therefore, the HUS rate in patients infected with group 1 EHEC was 28%, with group 2 EHEC was 67%, and with group 3 EHEC was 6%.

We did not isolate any EHEC strains from 126 of the 181 cases

TABLE 1 Numbers of patients in the groups defined by isolation of EHEC in stool specimens

Clinical presentation[a]	No. of patients in groups based on isolation of EHEC serotypes[b]				Total no.
	Group 1	Group 2	Group 3	Group 4	
HUS + AE, death	3	0	0	2	5
HUS + AE	4	6	0	6	16
HUS	2	2	1	8	13
Non-HUS[c]	16	4	17	110	147
Total no. of patients	25	12	18	126	181

[a] HUS, hemolytic uremic syndrome; AE, acute encephalopathy.
[b] Group 1, only EHEC O111 isolated from these patients; group 2, both EHEC O111 and EHEC O157 isolated from these patients; group 3, only EHEC O157 isolated from these patients; and group 4, neither EHEC O111 nor EHEC O157 isolated from these patients.
[c] More than one gastrointestinal symptom.

(Table 1, group 4). Of these 126 cases from group 4, 16 developed HUS, for an HUS rate of 13%, and 8 of these 16 HUS cases developed acute encephalopathy. In the serum samples of 10 patients of the 16 group 4 HUS cases, the anti-O111 antibody was detectable in all samples, whereas the antibody to O157 was only detectable in two samples. These data indicate that EHEC O111 isolates caused most infections, but these patients were no longer shedding EHEC (32).

An interesting feature of this outbreak was that *stx*-negative *E. coli* O111 strains were isolated from patient stool specimens. In addition, EHEC O157 strains with several types of toxins were isolated. These results are summarized in Table 2. *stx*-negative *E.*

TABLE 2 Profiles of serotypes and toxins of EHEC strains isolated from outbreak patients

Group[a]	No. of cases	Serogroup O111		Serogroup O157		
		stx_2	*stx*−	stx_1 stx_2	stx_1	stx_2
1	10	+[b]	−[b]	−	−	−
	15	+	+	−	−	−
2	5	+	+	+	−	−
	2	+	+	+	+	−
	3	+	−	+	−	−
	1	+	−	+	−	+
	1	+	+	−	+	−
3	3	−	+	+	−	−
	2	−	+	+	+	−
	5	−	−	+	−	−
	1	−	−	+	+	−
	3	−	−	+	−	+
	4	−	−	−	+	−
4	102	−	−	−	−	−
	24	−	+	−	−	−
Total no. of positive isolates		37	52[c]	25	10	4

[a] Groups 1 to 4 are defined in the Table 1 footnotes.
[b] Symbols indicate that the strain was isolated (+) or not isolated (−).
[c] Of these 52 isolates, 3 were not available and were therefore excluded from further analysis.

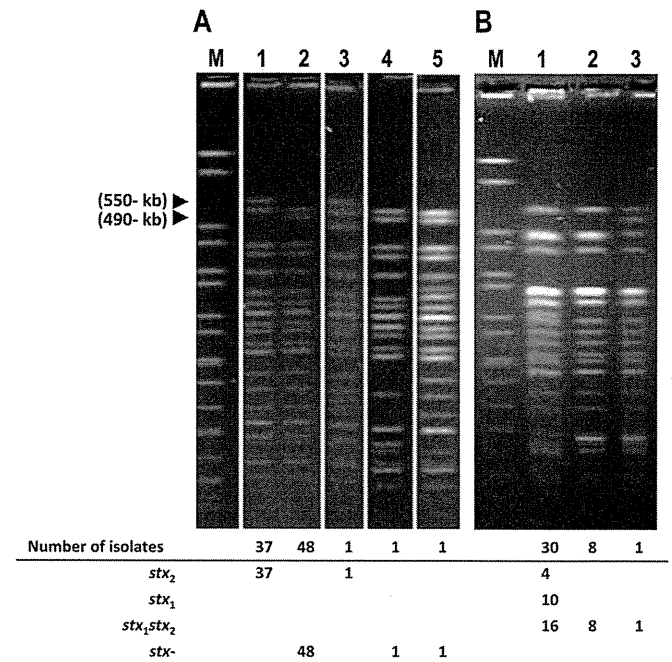

FIG 1 PFGE patterns of the *E. coli* O111 and *E. coli* O157 isolates and toxin types present. (A) Serogroup O111 isolates: lanes 1 and 3, stx_2-positive strains; lanes 2, 4, and 5, *stx*-negative strains. (B) Serogroup O157 isolates: lane 1, 16 stx_1 stx_2, 10 stx_1, and four stx_2-positive strains: lane 2, eight stx_1 stx_2-positive strains; lane 3, one stx_1 stx_2-positive strain. Each lane shows a representative PFGE pattern for each strain derived from the photographs of the separated gels. The tables in panels A and B show the number of strains with identical PFGE patterns and list a breakdown of the number of strains with each toxin type. Lane M, molecular markers; *stx*−, *stx*-negative.

coli O111 organisms were isolated from 28 of the 55 EHEC-positive cases (groups 1, 2, and 3) and from 24 of the 126 EHEC-negative cases (group 4). Further analysis was carried out on 37 EHEC O111 stx_2, 49 *stx*-negative *E. coli* O111, 25 EHEC O157 stx_1, 10 EHEC O157 stx_2, and 4 EHEC O157 stx_1 stx_2 strains, in addition to an EHEC O111 stx_2 and a *stx*-negative *E. coli* O111 isolate from a beef sample from the same lot as the suspected contaminated food, the raw beef dish yukhoe.

Molecular typing of *E. coli* isolates. If an EHEC strain loses its Stx prophage during infection, the resulting strain is an *stx*-negative *eae*-positive strain. Therefore, PFGE molecular typing was carried out to investigate the genetic relationships between the *stx*-positive and -negative EHEC O111 strains in this study. The PFGE patterns are shown in Fig. 1. All EHEC O111 stx_2 strains, including an isolate from a beef sample, had the same XbaI digestion pattern (Fig. 1A, lane 1), except one strain that had a similar pattern but with a three-band difference (Fig. 1A, lane 3). Of the 50 *stx*-negative EHEC O111 strains, 48 (96%), including an isolate from a beef sample, had the pattern shown in Fig. 1A, lane 2. There was only a two-band difference between the patterns of almost all *stx*-positive and -negative EHEC O111 strains (cf. Fig. 1A, lanes 1 and 2). A comparison of these PFGE patterns identified an approximately 550-kb band in *stx*-positive EHEC O111 strains that was not present in the patterns of *stx*-negative EHEC O111 strains, as well as an approximately 490-kb band in *stx*-negative EHEC O111 strains that was not present in the patterns of *stx*-positive EHEC O111 strains. The size difference of these bands, 60 kb, corresponds to the genome size of Stx-converting phages (33).

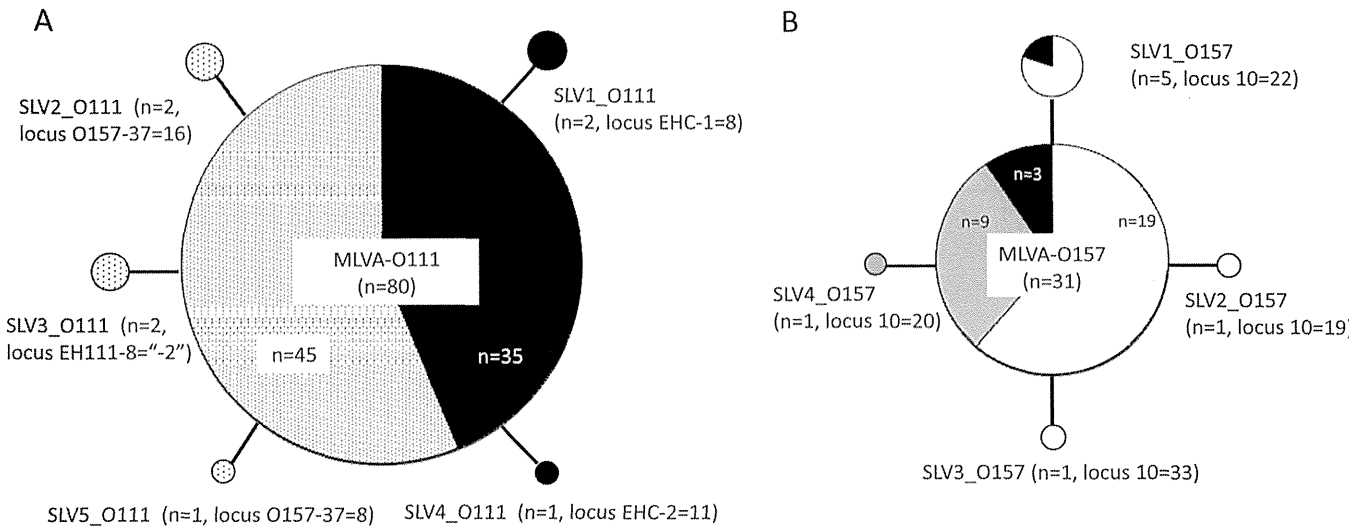

MLVA profile of MLVA-O111

Locus	EH 111 -11	EH 111 -14	EH 111 -8	EH 157 -12	EH 26 -7	EHC -1	EHC -2	EHC -5	EHC -6	O157-10	O157-17	O157-19	O157-25	O157 34	O157-36	O157-37	O157-3	O157-9
Repeat no.	4	1	5	3	-2	9	10	-2	3	-2	-2	1	2	3	-2	12	-2	11

MLVA profile of MLVA-O157

Locus	25	3	34	9	17	19	36	37	10
Repeat no.	4	5	9	18	7	4	12	7	21

FIG 2 Minimum spanning trees of MLVA of the *E. coli* O111 and *E. coli* O157 isolates. Shown are serogroup O111 isolates with stx_2 (black circle) or *stx*-negative *E. coli* (circle with dots) (A) and serogroup O157 isolates with stx_1 stx_2 (white circle), stx_1 (gray circle), or stx_2 (black circle) (B). One circle represents one MLVA type, and the size of the circle is proportional to the number of isolates. The tables in panels A and B show the MLVA profiles for *E. coli* O111 and *E. coli* O157 strains, with the gray columns indicating the locus detected single-locus variants (SLVs). Each SLV represents each satellite circle with the number of isolates and its locus type.

To confirm the genetic relationship of the EHEC O111 isolates from the outbreak, MLVA was carried out. Of the 88 *E. coli* O111 isolates, including the isolate from a beef sample, 80 (including both *stx*-positive and -negative isolates) had an identical MLVA profile. The remaining eight EHEC O111 isolates had similar MLVA profiles, but each had a repeat number variation at one locus among the 18 loci. These data strongly suggest that the *E. coli* O111 strains isolated during this outbreak were genetically closely related. The isolates from beef had a PFGE type (Fig. 1A, lane 1) and MLVA type (MLVA-O111) that appeared to be identical to those of the most prevalent *stx*-positive and -negative *E. coli* O111 isolates from clinical specimens, supporting the hypothesis that yukhoe beef was the vehicle for this outbreak.

The EHEC O157 isolates in this study were also analyzed by PFGE and MLVA to investigate the genetic relatedness of the three different toxin types present in these strains. There were three groups of EHEC O157 isolates based on a PFGE analysis of their XbaI restriction digest patterns, with one- to three-band differences (Fig. 1B). Of the 39 O157 isolates, 30 showed an identical PFGE pattern (Fig. 1B, lane 1). This pattern was found in all the EHEC O157 isolates carrying stx_1 stx_2, stx_1, and stx_2. An analysis of the MLVA results showed that the 39 EHEC O157 strains could be divided into five MLVA types (Fig. 2B). MLVA-O157 was the most commonly found MLVA type in 31 of the 39 strains and included strains with all three toxin types: stx_1 stx_2, stx_1, and stx_2. The remaining eight EHEC O157 strains were single-locus variants of MLVA-O157, each with a repeat number variation at locus 10 (see Fig.2, table for *E. coli* O157 in Fig. 2). Therefore, although EHEC O157 strains possessing different toxin types were isolated during this outbreak, all of the strains may have originated from a single common strain.

Shiga toxin production and other virulence markers. This outbreak produced an extraordinary number of cases of HUS and encephalopathy. In this outbreak, proinflammatory cytokines were induced in most patients with acute encephalopathy and severe HUS (34, 35). In addition to *E. coli* LPS, Stx1 and Stx2 can induce expression and synthesis of cytokines in Caco-2 cells, a human colon epithelial cell line (36). Therefore, we attempted to estimate the amount of Stx1 and Stx2 present in the culture media of EHEC strains isolated from outbreak patients. The 8 isolates of EHEC O111 stx_2 and 3 isolates of EHEC O157 stx_1 stx_2 produced Stx2 titers of 1:64 and 1:32, respectively, which were lower than those produced by EHEC O111 strain 11128 and EHEC O157 strain Sakai (1:128 and 1:256, respectively). The Stx1 titer of the EHEC O157 stx_1 stx_2 strains was also lower than that of the EHEC O157 strain Sakai (1:32 versus 1:128).

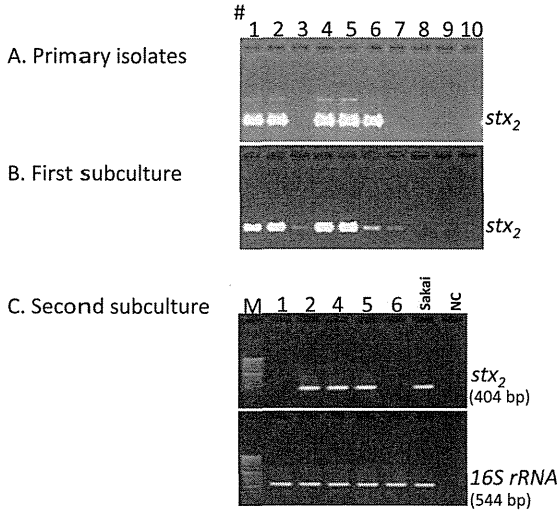

FIG 3 Stability of stx_2 genes of the five EHEC O111 stx_2 strains in successive subcultures. Ten O111 colonies (1 to 10) isolated from a stool specimen were picked, and each colony was spread on a TSA plate (A). A portion of each overnight subculture was transferred to a new TSA plate, and then this procedure was repeated to produce two subcultures. Following overnight incubation, the subcultures were tested using colony-sweep PCR for stx_2 (A, B, and C), and the five stx_2-positive colonies (1, 2, 4, 5, and 6) from the primary isolates were selected for the second round of subculture (C). The stx_2 and 16S rRNA gene amplicons were 404 bp and 544 bp, respectively. Sakai, EHEC O157 stx_1 stx_2 Sakai strain as a positive control; NC, template DNA-free reaction as a negative control.

To investigate additional potential virulence factors, like the hybrid type of STEC isolated in Germany in 2011 (36), the presence of major diarrheagenic *E. coli* virulence factors was examined by PCR. EHEC O111 stx_2, toxin-negative *E. coli*, and EHEC O157 isolates carried *eae*, *hlyA*, and *ospG* but were negative for CVD432, *aggR*, *invE*, *elt*, *esth*, *bfp*, EAF, and *astA* (data not shown). EHEC O111 strains had an intact *norV* gene, but EHEC O157 strains had a deletion in the *norV* gene (data not shown).

Furthermore, PCR subtyping of the Stx1 and Stx2 toxins from both the EHEC O111 and O157 strains in this outbreak showed that the toxins were types Stx1a and Stx2a.

Stability of the stx_2 gene during EHEC subculture. The EHEC isolates from some clinical specimens appeared to have lost the stx_2 gene during isolation and growth on the agar plates. For some EHEC O111 strains, we noted that the PFGE patterns, which were confirmed by PCR to be stx_2 positive, sometimes changed to the PFGE pattern of *stx*-negative *E. coli* O111 strains. To investigate the stability of the Stx2 prophage, 10 O111 colonies (1 to 10) isolated from a stool specimen were picked, and each colony was spread on a TSA plate. A portion of each overnight subculture was transferred to a new TSA plate, and then this procedure was repeated to produce two subcultures. After the overnight culture, the subcultures were tested using colony-sweep PCR for stx_2, and the five stx_2-positive colonies were selected from the primary isolates for the second subculture (Fig. 3). After the first subculture, the amount of PCR amplicon produced from isolate 6 was less than that produced from the other isolates. After the second subculture, no PCR stx_2 amplicon was seen in two of the five isolates (Fig. 3, isolates 1 and 6). The *E. coli* O111 strain, which converted to stx_2 negative in this experiment, had a PFGE pattern that was identical to that of the *stx*-negative *E. coli* O111 strains (data not shown), indicating that an Stx2 prophage had been lost during subculture. Collectively, these data indicate that some Stx2 prophages in the EHEC O111 strains isolated in this outbreak were unstable during *in vitro* cultivation, and they suggest that loss of the Stx2 prophage may have occurred in the infected patients.

DISCUSSION

Several reports have identified EHEC-associated HUS cases that no longer shed EHEC but do shed *stx*-negative EHEC organisms that presumably lost *stx* during infection (18, 37–39). Stx is the most important EHEC virulence factor, causing the specific clinical features of EHEC infection (1–4). Therefore, *stx*-negative *E. coli* organisms may be produced by excision of the Stx-converting phage during infection. In agreement with this suggestion, more *stx*-negative EHEC strains have been isolated at follow-up testing of EHEC-infected patients (38). In HUS patients who shed only *stx*-negative EHEC, the etiology of HUS can be missed using current bacteriological methods based on detecting only the *stx* gene or Stx. This can hamper epidemiological investigations and lead to inappropriate clinical management, especially with a cluster of sporadic cases.

The etiology of the EHEC O111/O157 outbreak studied here was confirmed in only 18 of the 34 HUS cases by isolating EHEC O111 (9 cases), EHEC O157 (1 case), and both EHEC O111 and O157 (8 cases). The remaining 16 HUS cases were EHEC negative, even after extensive efforts to isolate EHEC, with up to 800 *E. coli* colonies examined after O111 enrichment using immunomagnetic beads. Since serologically positive results for the *E. coli* O111 antigen were found from all but one of the EHEC-negative HUS cases (32), EHEC O111 may be the primary cause of the severe HUS complications. An *stx*-negative *E. coli* O111 strain was isolated from most EHEC-positive HUS cases (13 of 18 HUS cases) and from a few EHEC-negative HUS cases (3 of 16 HUS cases). We also isolated EHEC O111 stx_2 and *stx*-negative *E. coli* O111 organisms from a beef sample from the same lot as the suspected infection vehicle. Therefore, conversion from *stx*-positive to *stx*-negative *E. coli* O111 may occur in contaminated food, during infection, and/or bacteriological testing. The subculture data presented here show that the EHEC O111 stx_2 isolates in this study can lose the Stx2 prophage during *in vitro* subculture (Fig. 3). This may have biased our bacteriological analyses, resulting in an underestimation of the scale of the outbreak. Since the loss of the *stx* gene was not consistent in all EHEC O111 isolates in this study, with some isolates remaining stx_2 positive during subculture and other isolates losing stx_2, the molecular mechanism and factors affecting the loss of the stx_2 phage require further study.

Bielaszewka et al. (40) reported the isolation of *stx*-negative EHEC organisms from approximately 5% of the HUS patients. In that report, the majority of the *stx*-negative/*eae*-positive isolates belonged to serogroups O26, O103, O145, and O157:H7/NM, but no *stx*-negative/*eae*-positive *E. coli* O111 isolates were reported. The absence of *stx*-negative/*eae*-positive *E. coli* O111 isolates in the HUS patients may be explained by the fact that a majority of the EHEC O111 isolates possessed stx_1 solely or in combination with stx_2 (13), and the Stx1 prophage of EHEC O111 is thought to be defective, resulting in immobilization and stability in the EHEC chromosome (41). In contrast to a previous investigation (39), there were 16 HUS cases (47.1% [16 in 34 HUS cases]) in this outbreak from patients whose stools contained *stx*-negative *E. coli*

O111 strains. It is probably because EHEC O111 in this outbreak possessed the Stx2 prophage only, which was unstable and progressively lost from the genome. An HUS outbreak in Italy in 1992 may have involved a similar loss of Stx phages during EHEC O111 infection (15). That HUS outbreak had nine HUS cases, including 6 cases that were diagnosed by detecting a serum antibody to *E. coli* O111 LPS. Stx-producing *E. coli* was isolated from a stool specimen in only one case. Unfortunately, there were no data on the isolation of *stx*-negative strains.

The prevalence of HUS (19% [34 of 181 EHEC-infected patients]) was unexpectedly high in the 2011 outbreak, even if the suspected cases are included in the calculation. The most probable explanation for this relatively high HUS prevalence is that the concentration of EHEC in the EHEC-contaminated food was high. However, the EHEC O111 and EHEC O157 concentrations in the vehicles for the outbreak studied here are not known. We were unable to examine the raw beef dish, yukhoe, which was the vehicle for EHEC O111, and thus far, the vehicle for EHEC O157 has not been confirmed. The cytokine profiles of the patients with serious complications in this outbreak indicate that massive induction of proinflammatory cytokines may have contributed to the development of serious complications (34, 35). The high level of cytokine induction may have been due to LPS release in the intestinal tract, although it remains unclear how LPS-dependent induction might have occurred in this outbreak. In addition, although Stx1 and Stx2 may induce cytokines, including tumor necrosis factor alpha, the amount of Stx2 production in the EHEC O111 strains, as well as Stx1 and Stx 2 production in the EHEC O157 strains, in this outbreak was low or similar to that in EHEC O111 strain 11128 and EHEC O157 Sakai by *in vitro* testing. Unfortunately, we did not determine the reasons for this high HUS prevalence using the *in vitro* bacteriological testing alone. Another possibility is that the instability of the Stx2 prophages in the EHEC O111 strains may have played a role in the high HUS prevalence in this outbreak. Mellmann et al. (42) suggested that *stx*-negative EHEC strains might be the recipients of Stx-converting phages from isogenic *stx*-positive strains. In fact, we detected many Stx2 phage plaques in the culture lysates of some EHEC O111 isolates following incubation with mitomycin C, as well as in some of the bloody stool specimens (data not shown). Almost all of these plaques were shown to be stx_2 positive by the PCR assay, and these phages were found to be functional Stx2-converting phages. This would suggest a highly dynamic system that converts in both directions by the loss or gain of Stx2 phages. This cycling lifestyle might be enhanced by a mixture of *stx*-positive EHEC organisms and its isogenic *stx*-negative strain in the contaminated vehicle or during infection. Further studies of integrated prophages in both the EHEC O111 and EHEC O157 strains isolated during this outbreak need to be carried out, because the dynamic conversion of these strains might influence the outcome of disease.

ACKNOWLEDGMENTS

We thank the public health centers of Takaoka, Tonami, and Toyama City, the medical laboratories of Tonami General Hospital, Kouseiren Takaoka Hospital, Takaoka City Hospital, and Toyama University Hospital for collecting clinical specimens during the 2011 EHEC outbreak, and Yoshihiro Takada of the Toyama Institute of Health for continuing encouragement in this study.

This work was supported by a Special Research grant (H23-TOKU-BETU-SHITEI-004 and H24-SHINKO-IPPAN-012) and a Health Labor Sciences Research grant from the Ministry of Health, Labor, and Welfare, Japan.

We declare that we have no conflicts of interest.

REFERENCES

1. O'Brien AD, Kaper JB. 1998. Shiga toxin-producing *Escherichia coli*: yesterday, today, and tomorrow, p 1–11. *In* Kaper JB, O'Brien AD (ed), *Escherichia coli* O157:H7 and other Shiga toxin-producing *E. coli* strains. ASM Press, Washington, DC.
2. Nataro JP, Kaper JB. 1998. Diarrheagenic *Escherichia coli*. Clin. Microbiol. Rev. 11:142–201.
3. Karmali MA, Steele BT, Petric M, Lim C. 1983. Sporadic cases of haemolytic-uraemic syndrome associated with faecal cytotoxin and cytotoxin-producing *Escherichia coli* in stools. Lancet 321:619–620. http://dx.doi.org/10.1016/S0140-6736(83)91795-6.
4. Mayer CL, Leibowitz CS, Kurosawa S, Stearns-Kurosawa DJ. 2012. Shiga toxins and the pathophysiology of hemolytic uremic syndrome in humans and animals. Toxins (Basel) 4:1261–1287. http://dx.doi.org/10.3390/toxins4111261.
5. National Institute of Infectious Diseases. 2013. Enterohemorrhagic *Escherichia coli* infection in Japan as of April 2013. IASR 34:123–124. http://www.nih.go.jp/niid/en/iasr-vol34-e/865-iasr/3570-tps399.html.
6. National Institute of Infectious Diseases. 2007. Enterohemorrhagic *Escherichia coli* infection in Japan as of April 2007. IASR 28:131–132. http://idsc.nih.go.jp/iasr/28/327/tpc327.html.
7. National Institute of Infectious Diseases. 2008. Enterohemorrhagic *Escherichia coli* infection in Japan as of April 2008. IASR 29:117–118. http://idsc.nih.go.jp/iasr/29/339/tpc339.html.
8. National Institute of Infectious Diseases. 2009. Enterohemorrhagic *Escherichia coli* infection in Japan as of April 2009. IASR 30:119–120. http://idsc.nih.go.jp/iasr/30/351/tpc351.html.
9. National Institute of Infectious Diseases. 2010. Enterohemorrhagic *Escherichia coli* infection in Japan as of May 2010. IASR 31:151–152. http://idsc.nih.go.jp/iasr/31/364/tpc364.html.
10. National Institute of Infectious Diseases. 2011. Enterohemorrhagic *Escherichia coli* infection in Japan as of April 2011. IASR 32:125–126. http://idsc.nih.go.jp/iasr/32/375/tpc375.html.
11. Brooks JT, Sowers EG, Wells JG, Greene KD, Griffin PM, Hoekstra RM, Strockbine NA. 2005. Non-O157 Shiga toxin-producing *Escherichia coli* infections in the United States, 1983–2002. J. Infect. Dis. 192:1422–1429. http://dx.doi.org/10.1086/466536.
12. Beutin L, Krause G, Zimmermann S, Kaulfuss S, Gleier K. 2004. Characterization of Shiga toxin-producing *Escherichia coli* strains isolated from human patients in Germany over a 3-year period. J. Clin. Microbiol. 42:1099–1108. http://dx.doi.org/10.1128/JCM.42.3.1099-1108.2004.
13. Zhang W, Mellmann A, Sonntag AK, Wieler L, Bielaszewska M, Tschäpe H, Karch H, Friedrich AW. 2007. Structural and functional differences between disease-associated genes of enterohaemorrhagic *Escherichia coli* O111. Int. J. Med. Microbiol. 297:17–26. http://dx.doi.org/10.1016/j.ijmm.2006.10.004.
14. Elliott EJ, Robins-Browne RM, O'Loughlin EV, Bennett-Wood V, Bourke J, Henning P, Hogg GG, Knight J, Powell H, Redmond D, Contributors to the Australian Paediatric Surveillance Unit. 2001. Nationwide study of haemolytic uraemic syndrome: clinical, microbiological, and epidemiological features. Arch. Dis. Child. 85:125–131. http://dx.doi.org/10.1136/adc.85.2.125.
15. Caprioli A, Luzzi I, Rosmini F, Resti C, Edefonti A, Perfumo F, Farina C, Goglio A, Gianviti A, Rizzoni G. 1994. Community-wide outbreak of hemolytic uremic syndrome associated with non-O157 verocytotoxin-producing *Escherichia coli*. J. Infect. Dis. 169:208–211. http://dx.doi.org/10.1093/infdis/169.1.208.
16. Piercefield EW, Bradley KK, Coffman RL, Mallonee SM. 2010. Hemolytic uremic syndrome after an *Escherichia coli* O111 outbreak. Arch. Intern. Med. 170:1656–1663. http://dx.doi.org/10.1001/archinternmed.2010.346.
17. Karch H, Meyer T, Rüssmann H, Heesemann J. 1992. Frequent loss of Shiga-like toxin genes in clinical isolates of *Escherichia coli* upon subcultivation. Infect. Immun. 60:3464–3467.
18. Friedrich AW, Zhang W, Bielaszewska M, Mellmann A, Köck R, Fruth A, Tschäpe H, Karch H. 2007. Prevalence, virulence profiles, and clinical

significance of Shiga toxin-negative variants of enterohemorrhagic *Escherichia coli* O157 infection in humans. Clin. Infect. Dis. 45:39–45. http://dx.doi.org/10.1086/518573.

19. Ogura Y, Ooka T, Iguchi A, Toh H, Asadulghani M, Oshima K, Kodama T, Abe H, Nakayama K, Kurokawa K, Tobe T, Hattori M, Hayashi T. 2009. Comparative genomics reveal the mechanism of the parallel evolution of O157 and non-O157 enterohemorrhagic *Escherichia coli*. Proc. Natl. Acad. Sci. U. S. A. 106:17939–17944. http://dx.doi.org/10.1073/pnas.0903585106.
20. Hayashi T, Makino K, Ohnishi M, Kurokawa K, Ishii K, Yokoyama K, Han CG, Ohtsubo E, Nakayama K, Murata T, Tanaka M, Tobe T, Iida T, Takami H, Honda T, Sasakawa C, Ogasawara N, Yasunaga T, Kuhara S, Shiba T, Hattori M, Shinagawa H. 2001. Complete genome sequence of enterohemorrhagic *Escherichia coli* O157:H7 and genomic comparison with a laboratory strain K-12. DNA Res. 8:11–22. http://dx.doi.org/10.1093/dnares/8.1.11.
21. Karch H, Janetzki-Mittmann C, Aleksic S, Datz M. 1996. Isolation of enterohemorrhagic *Escherichia coli* O157 strains from patients with hemolytic-uremic syndrome by using immunomagnetic separation, DNA-based methods, and direct culture. J. Clin. Microbiol. 34:516–519.
22. Fukushima H, Hoshina K, Gomyda M. 2000. Selective isolation of *eae*-positive strains of Shiga toxin-producing *Escherichia coli*. J. Clin. Microbiol. 38:1684–1687.
23. Beutin L, Strauch E. 2007. Identification of sequence diversity in the *Escherichia coli fliC* genes encoding flagellar types H8 and H40 and its use in typing of Shiga toxin-producing *E. coli* O8, O22, O111, O174 and O179 strains. J. Clin. Microbiol. 45:333–339. http://dx.doi.org/10.1128/JCM.01627-06.
24. Hunter SB, Vauterin P, Lambert-Fair MA, Van Duyne MS, Kubota K, Graves L, Wrigley D, Barrett T, Ribot E. 2005. Establishment of a universal size standard strain for use with the PulseNet standardized pulsed-field gel electrophoresis protocols: converting the national databases to the new size standard. J. Clin. Microbiol. 43:1045–1050. http://dx.doi.org/10.1128/JCM.43.3.1045-1050.2005.
25. Izumiya H, Pei Y, Terajima J, Ohnishi M, Hayashi T, Iyoda S, Watanabe H. 2010. New system for multilocus variable-number tandem-repeat analysis of the enterohemorrhagic *Escherichia coli* strains belonging to three major serogroups: O157, O26, and O111. Microbiol. Immunol. 54:569–577. http://dx.doi.org/10.1111/j.1348-0421.2010.00252.x.
26. Hyytiä-Trees E, Smole SC, Fields PA, Swaminathan B, Ribot E. 2006. Second generation subtyping: a proposed PulseNet protocol for multiple-locus variable-number tandem repeat analysis of Shiga toxin-producing *Escherichia coli* O157 (STEC O157). Foodborne Pathog. Dis. 3:118–131. http://dx.doi.org/10.1089/fpd.2006.3.118.
27. Walsh PS, Metzger DA, Higuchi R. 1991. Chelex 100 as a medium for simple extraction of DNA for PCR-based typing from forensic material. Biotechniques 10:506–513.
28. Kimata K, Shima T, Shimizu M, Tanaka D, Isobe J, Gyobu Y, Watahiki M, Nagai Y. 2005. Rapid categorization of pathogenic *Escherichia coli* by multiplex PCR. Microbiol. Immunol. 49:485–492. http://dx.doi.org/10.1111/j.1348-0421.2005.tb03752.x.
29. Scheutz F, Teel LD, Beutin L, Piérard D, Buvens G, Karch H, Mellmann A, Caprioli A, Tozzoli R, Morabito S, Strockbine NA, Melton-Celsa AR, Sanchez M, Persson S, O'Brien AD. 2012. Multicenter evaluation of a sequence-based protocol for subtyping Shiga toxins and standardizing Stx nomenclature. J. Clin. Microbiol. 50:2951–2963. http://dx.doi.org/10.1128/JCM.00860-12.
30. Kulasekara BR, Jacobs M, Zhou Y, Wu Z, Sims E, Saenphimmachak C, Rohmer CL, Ritchie JM, Radey M, McKevitt M, Freeman TL, Hayden H, Haugen E, Gillett W, Fong C, Chang J, Beskhlebnaya V, Waldor MK, Samadpour M, Whittam TS, Kaul R, Brittnacher M, Miller SL. 2009. Analysis of the genome of the *Escherichia coli* O157:H7 2006 spinach-associated outbreak isolate indicates candidate genes that may enhance virulence. Infect. Immun. 77:3713–3721. http://dx.doi.org/10.1128/IAI.00198-09.
31. Nobe R, Nougayrède JP, Taieb F, Bardiau M, Cassart D, Navarro-Garcia F, Mainil J, Hayashi T, Oswald E. 2009. Enterohaemorrhagic *Escherichia coli* serogroup O111 inhibits NF-κB-dependent innate responses in a manner independent of a type III secreted OspG orthologue. Microbiology 155:3214–3225. http://dx.doi.org/10.1099/mic.0.030759-0.
32. Isobe J, Shima T, Kanatani J, Kimata K, Shimizu M, Kobayashi N, Tanaka T, Iyoda S, Ohnishi M, Sata T, Watahiki M. 2014. Serodiagnosis using microagglutination assay during the food-poisoning outbreak in Japan caused by consumption of raw beef contaminated with enterohemorrhagic *Escherichia coli* O111 and O157. J. Clin. Microbiol. 52:1112–1118. http://dx.doi.org/10.1128/JCM.03469-13.
33. Plunkett G, III, Rose DJ, Durfee TJ, Blattner FR. 1999. Sequence of Shiga toxin 2 phage 933W from *Escherichia coli* O157:H7: Shiga toxin as a phage late-gene product. J. Bacteriol. 181:1767–1678.
34. Shimizu M, Kuroda M, Sakashita N, Konishi M, Kaneda H, Igarashi N, Yamahana J, Taneichi H, Kanegane H, Ito M, Saito S, Ohta K, Taniguchi T, Furuichi K, Wada T, Nakagawa M, Yokoyama H, Yachie A. 2012. Cytokine profiles of patients with enterohemorrhagic *Escherichia coli* O111-induced hemolytic-uremic syndrome. Cytokine 60:694–700. http://dx.doi.org/10.1016/j.cyto.2012.07.038.
35. Shimizu M, Kuroda M, Inoue N, Konishi M, Igarashi N, Taneichi H, Kanegane H, Ito M, Saito S, Yachie A. 2014. Extensive serum biomarker analysis in patients with enterohemorrhagic *Escherichia coli* O111-induced hemolytic-uremic syndrome. Cytokine 66:1–6. http://dx.doi.org/10.1016/j.cyto.2013.12.005.
36. Yamasaki C, Natori Y, Zeng XT, Ohmura M, Yamasaki S, Takeda Y, Natori Y. 1999. Induction of cytokines in a human colon epithelial cell line by Shiga toxin 1 (Stx1) and Stx2 but not by non-toxic mutant Stx1 which lacks *N*-glycosidase activity. FEBS Lett. 442:231–234. http://dx.doi.org/10.1016/S0014-5793(98)01667-6.
37. Bielaszewska M, Mellmann A, Zhang W, Köck R, Fruth A, Bauwens A, Peters G, Karch H. 2011. Characterisation of the *Escherichia coli* strain associated with an outbreak of haemolytic uraemic syndrome in Germany, 2011: a microbiological study. Lancet Infect. Dis. 11:671–676. http://dx.doi.org/10.1016/S1473-3099(11)70165-7.
38. Feng P, Dey M, Abe A, Takeda T. 2001. Isogenic strain of *Escherichia coli* O157:H7 that has lost both Shiga toxin 1 and 2 genes. Clin. Diagn. Lab. Immunol. 8:711–717.
39. Mellmann A, Bielaszewska M, Zimmerhackl LB, Prager R, Harmsen D, Tschäpe H, Karch H. 2005. Enterohemorrhagic *Escherichia coli* in human infection: *in vivo* evolution of a bacterial pathogen. Clin. Infect. Dis. 41:785–792. http://dx.doi.org/10.1086/432722.
40. Bielaszewska M, Köck R, Friedrich AW, von Eiff C, Zimmerhackl LB, Karch H, Mellmann A. 2007. Shiga toxin-mediated hemolytic uremic syndrome: time to change the diagnostic paradigm? PLoS One 2:e1024. http://dx.doi.org/10.1371/journal.pone.0001024.
41. Creuzburg K, Köhler B, Hempel H, Schreier P, Jacobs E, Schmidt H. 2005. Genetic structure and chromosomal integration site of the cryptic prophage CP-1639 encoding Shiga toxin. Microbiology 151:941–950. http://dx.doi.org/10.1099/mic.0.27632-0.
42. Mellmann A, Lu S, Karch H, Xu J, Harmsen D, Schmidt MA, Bielaszewska M. 2008. Recycling of Shiga toxin 2 genes in sorbitol-fermenting enterohemorrhagic *Escherichia coli* O157:NM. Appl. Environ. Microbiol. 74:67–72. http://dx.doi.org/10.1128/AEM.01906-07.

IAI
Journals.ASM.org

DAP1, a Negative Regulator of Autophagy, Controls SubAB-Mediated Apoptosis and Autophagy

Kinnosuke Yahiro,[a] Hiroyasu Tsutsuki,[a] Kohei Ogura,[a] Sayaka Nagasawa,[a,b] Joel Moss,[c] Masatoshi Noda[a]

Departments of Molecular Infectiology[a] and Legal Medicine,[b] Graduate School of Medicine, Chiba University, Chiba, Japan; Cardiovascular and Pulmonary Branch, National Heart, Lung, and Blood Institute, National Institutes of Health, Bethesda, Maryland, USA[c]

Autophagy and apoptosis play critical roles in cellular homeostasis and survival. Subtilase cytotoxin (SubAB), produced by non-O157 type Shiga-toxigenic *Escherichia coli* (STEC), is an important virulence factor in disease. SubAB, a protease, cleaves a specific site on the endoplasmic reticulum (ER) chaperone protein BiP/GRP78, leading to ER stress, and induces apoptosis. Here we report that in HeLa cells, activation of a PERK (RNA-dependent protein kinase [PKR]-like ER kinase)-eIF2α (α subunit of eukaryotic initiation factor 2)-dependent pathway by SubAB-mediated BiP cleavage negatively regulates autophagy and induces apoptosis through death-associated protein 1 (DAP1). We found that SubAB treatment decreased the amounts of autophagy markers LC3-II and p62 as well as those of mTOR (mammalian target of rapamycin) signaling proteins ULK1 and S6K. These proteins showed increased expression levels in PERK knockdown or DAP1 knockdown cells. In addition, depletion of DAP1 in HeLa cells dramatically inhibited the SubAB-stimulated apoptotic pathway: SubAB-induced Bax/Bak conformational changes, Bax/Bak oligomerization, cytochrome *c* release, activation of caspases, and poly(ADP-ribose) polymerase (PARP) cleavage. These results show that DAP1 is a key regulator, through PERK-eIF2α-dependent pathways, of the induction of apoptosis and reduction of autophagy by SubAB.

Shiga-toxigenic *Escherichia coli* (STEC) infection causes gastrointestinal disease, including diarrhea, hemorrhagic colitis (1), and hemolytic-uremic syndrome (HUS) (1–3). The bacterial products Shiga toxins 1 and 2 are important virulence factors in the pathogenesis of disease (4). In addition, subtilase cytotoxin (SubAB) was discovered in STEC O113:H21 strain 98NK2, which was responsible for an outbreak of HUS (5). SubAB is produced primarily by a variety of non-O157 serotypes of STEC; STEC O157:H7, the most common serogroup implicated in hemorrhagic colitis and HUS, almost never produces SubAB (6–9). SubAB has an enzymatically active subunit, which is a subtilase-like serine protease, and five receptor recognition domains, which play important roles in binding to the receptor on the target cell surface (5).

In order to understand SubAB cytotoxicity, it was investigated in cultured cells. First, it was observed that SubAB bound to surface receptors (e.g., Neu5Gc [10]), shown to be terminally sialic acid modified membrane proteins (11, 12), and was translocated into target cells. After being endocytosed, SubAB was transported to the Golgi apparatus, which was confirmed by its colocalization with golgin-97, a marker protein of the Golgi apparatus. SubAB was delivered to the endoplasmic reticulum (ER) via a COG (conserved oligomeric Golgi)/Rab6/COPI (coat protein I)-dependent pathway (13). In the ER, SubAB cleaves a specific site at Leu416 on endoplasmic reticulum chaperone BiP/GRP78 (14). SubAB-dependent BiP cleavage is inhibited by brefeldin A (BFA), a Golgi complex-disrupting agent (15, 16). SubAB-induced ER stress due to BiP cleavage causes activation of stress sensor proteins, followed by the induction of various cellular events leading to cell damage, e.g., transient inhibition of protein synthesis (17), G_0/G_1 cell cycle arrest (15, 17), caspase-dependent apoptosis via mitochondrial membrane damage (18), activation of Akt-NF-κB signaling (19), downregulation of gap junction expression (20), activation of RNA-dependent protein kinase (PKR)-like ER kinase (PERK) followed by caspase-dependent apoptosis (12), and inhibition of lipopolysaccharide (LPS)-stimulated NO production through inhibition of NF-κB nuclear translocation and inducible nitric oxide synthase (iNOS) expression (21).

Macroautophagy (referred to below as autophagy) is mediated by autophagosomes, double-membrane vesicles that enclose a portion of the cytoplasm for delivery to the lysosome. Autophagosome formation is dynamically regulated by starvation and other stresses and involves complicated membrane reorganization (22). Recent studies have shown that autophagy is an important component of the innate defense against a variety of infectious agents. Microorganisms, however, have evolved strategies for evading or subverting host autophagy so as to survive and establish persistent infections (23, 24). In addition, there are negative regulators of autophagy (e.g., HO-1, Nrf2) (25–27). Death-associated protein 1 (DAP1) has been identified as a novel substrate of mammalian target of rapamycin (mTOR) that negatively regulates autophagy (28). DAP1 (15 kDa) was initially identified for its role in programmed cell death (29) and was shown to be ubiquitously expressed in many types of cells and tissues (30). We show here the molecular mechanisms involved in SubAB-mediated suppression of the generation of autophagy marker LC3-II, including reduced expression levels of factors of autophagy. We observed that DAP1 was a key factor in the regulation of SubAB-induced apoptosis and autophagy.

Received 16 June 2014 Returned for modification 11 July 2014
Accepted 25 August 2014
Published ahead of print 2 September 2014
Editor: B. A. McCormick
Address correspondence to Kinnosuke Yahiro, yahirok@faculty.chiba-u.jp.

doi:10.1128/IAI.02213-14

MATERIALS AND METHODS

Subtilase cytotoxin preparation. *Escherichia coli* producing recombinant His-tagged wild-type (wt) subtilase cytotoxin (SubAB) or catalytically inactivated mutant (mt) SubAB (with an S272A alteration in SubA) was used as the source of toxins for purification according to a published procedure (17).

Antibodies and other reagents. Antibodies against Atg5, Atg7, Atg12, Atg16L1, Beclin 1, DAP1, eIF2α, phospho-eIF2α(Ser51), LC3B, ULK1, phospho-ULK1(Ser757), p70 S6 kinase (S6K), phospho-S6K(Thr389), cleaved caspase-7 (cCas7), cleaved poly(ADP-ribose) polymerase (cPARP), PERK, SQTMT1/p62, mTOR, and phospho-mTOR(S2448) were purchased from Cell Signaling. Mouse monoclonal antibodies against BiP/GRP78 were from BD Biosciences, and the antibody against glyceraldehyde-3-phosphate dehydrogenase (GAPDH) was from GeneTex. The anti-LC3 monoclonal antibody (clone 1703) was from Cosmo Bio; Z-Val-Ala-Asp-fluoromethylketone (Z-VAD-FMK) was from R&D Systems; Necrostatin-1 and the anti-α-tubulin antibody were from Sigma-Aldrich; 3-methyladenine (3-MA) was from MP Biomedicals; and bafilomycin A1 (Baf A1) and cycloheximide were from Wako.

Cell culture and gene transfection. HeLa cells were cultured in Earle's minimal essential medium (Sigma) containing 10% fetal calf serum (FCS). Cells were plated into 24-well dishes (5×10^4 cells/well) or 12-well dishes (1×10^5 cells/well) with medium containing 10% FCS. RNA interference-mediated gene knockdown was performed using validated Qiagen HP small interfering RNAs (siRNAs) for Atg12 (SI02655289) and PERK (SI02223718). The Atg16L1 siRNA (5′-CAGGACAATGTGGATA CTCAT-3′) was designed and validated as described previously (31). SQSTM1/p62 siRNAs (5′-GUAAGCCUAGGUGUUGUCATT-3′) were designed and validated as described previously (32). DAP1 siRNAs were purchased from Dharmacon. Negative-control siRNAs were purchased from Sigma-Aldrich. Cells were transfected with siRNAs at 50 to 100 nM for 48 h by using Lipofectamine RNAiMax transfection reagent (Invitrogen) according to the manufacturer's protocol. The knockdown of the target proteins was confirmed by immunoblotting. The Myc-tagged hULK1 plasmid (33) was obtained from Addgene (plasmid 31961). HeLa cells were transfected with X-tremeGENE HP DNA transfection reagent (Roche) according to the manufacturer's instruction manual.

Cell viability assay. HeLa cells (1×10^4/well) were incubated with wild-type or catalytically inactive mutant SubAB (200 ng/ml) for the indicated times. Cell viability was measured by a Cell Counting kit (Dojindo) according to the manufacturer's instructions.

Immunoprecipitation. Conformationally changed Bax or Bak was coimmunoprecipitated as described previously (34). Briefly, the indicated siRNA-transfected HeLa cells were treated with wt or mt SubAB for 3 h. After a wash with ice-cold phosphate-buffered saline (PBS), cells were solubilized with lysis buffer {10 mM HEPES, 150 mM NaCl, 1.5 mM $MgCl_2$, 1 mM EGTA, 2% 3-[(3-cholamidopropyl)-dimethylammonio]-1-propanesulfonate [CHAPS] [pH 7.4]} containing protease inhibitor cocktail (Roche Diagnostics) and were incubated for 30 min on ice. After centrifugation at 17,400 × *g* for 15 min at 4°C, solubilized extracts (100 μg/200 μl) were collected and were incubated with a conformation-specific anti-Bax (clone 3; BD Bioscience) or anti-Bak (Ab-2; Calbiochem) antibody at 4°C for 3 h. Immunoprecipitates were collected by incubation with protein G-Sepharose (Invitrogen) for 1 h, followed by centrifugation for 1 min at 4°C. After immunocomplexes were washed three times with lysis buffer, proteins were dissolved in SDS sample buffer, subjected to SDS-PAGE in 15% gels, and transferred to polyvinylidene difluoride (PVDF) membranes, which were then analyzed by Western blotting using anti-Bax or anti-Bak antibodies (Cell Signaling).

Immunoblot analysis. Cell lysis and immunoblotting were performed as described previously (12). Briefly, proteins were separated by SDS-PAGE and were transferred to PVDF membranes, which were incubated with the indicated primary antibodies. Detection was performed with horseradish peroxidase-labeled goat anti-mouse or anti-rabbit secondary antibodies, followed by enhanced chemiluminescence (Super Signal; Pierce). Bands were visualized using a LAS-1000 system (Fujifilm). Densitometric analysis was performed by Image Gauge software (Fujifilm) on the scanned blots, and protein levels were normalized to those of α-tubulin or GAPDH.

Immunofluorescence confocal microscopy. For immunofluorescence analysis of LC3B or SQSTM1/p62, 1×10^5 HeLa cells on the microcoverglass (Matsunami) were incubated with 200 ng/ml wt or mt SubAB for the indicated times. Cells were fixed with 4% paraformaldehyde (PFA) at room temperature for 15 min, washed twice with PBS, and then immediately permeabilized with ice-cold 100% methanol for 10 min at −20°C. The cells were then rinsed three times with PBS and incubated with blocking buffer (5% goat serum, 0.3% Triton X-100 in PBS) at room temperature for 1 h. To visualize LC3B (D11; dilution, 1:200) or SQSTM1/p62 (D10E10; dilution, 1:400), cells were further incubated with primary antibodies in 0.4% bovine serum albumin (BSA)-PBS buffer at 4°C overnight, washed twice with PBS, and incubated with a DyLight 488-conjugated anti-mouse antibody (Rockland) or a Cy3-conjugated anti-rabbit antibody (Sigma) at room temperature for 1 h in the dark. After three washes with PBS, cells were mounted on glass slides using Prolong Gold Antifade reagent with 4′,6-diamidino-2-phenylindole (DAPI). The stained cells were visualized by FV10i-LIV confocal microscopy (Olympus). The images were arranged with Adobe Photoshop CS4.

Statistics. The *P* values for densitometric analysis and vacuolating assays were determined by Student's *t* test with GraphPad Prism software (GraphPad, San Diego, CA). *P* values of <0.05 were considered statistically significant.

RESULTS

SubAB negatively regulates autophagy in HeLa cells. To understand the relationship between autophagy and SubAB-induced apoptosis in HeLa cells, we examined the effect of SubAB on the conversion of LC3 and the expression level of p62. Studies have shown that during autophagosome formation, the level of autophagy marker LC3-II was increased and it accumulated in autophagosomal membranes, while the level of p62 was decreased in autophagosomes (35, 36). We first investigated the effect of SubAB on HeLa cell viability, which was significantly decreased after 48 h of incubation with wild-type (wt) SubAB, but not with catalytically inactive mutant (mt) SubAB (Fig. 1a). Although SubAB-induced caspase-7 activation was observed after 3 h of incubation, the amounts of LC3-II and p62 were decreased in a time-dependent manner (Fig. 1b). We next investigated the effects of SubAB on the classical mTOR pathway in HeLa cells. As shown in Fig. 1c, wt SubAB, but not mt SubAB, induced BiP cleavage within 1 h. SubAB treatment for 3 h suppressed ULK1 and S6K expression. Previous studies have shown that ULK1 is a regulator of autophagy (33). Therefore, we examined the effect of transient expression of ULK1 in HeLa cells on the inhibition of LC3-II generation by SubAB. Compared with control plasmid-transfected cells, ULK1 overexpression did not inhibit the suppression of LC3-II and p62 by SubAB (Fig. 1d). Further, we also investigated the effect of ULK1 overexpression on SubAB-induced apoptosis. As shown in Fig. 1e, overexpression of ULK1 did not affect SubAB-induced PERK phosphorylation, eIF2α phosphorylation, caspase-7 activation, or PARP cleavage. These data suggest that SubAB functions independently of ULK1.

SubAB suppression of autophagy is required for PERK-mediated signaling. Previously, we demonstrated that SubAB induction of apoptosis by BiP cleavage was mediated by the ER stress sensor protein PERK (12). Therefore, we next investigated if PERK-related signaling pathways were associated with SubAB suppression of autophagy in HeLa cells. We determined the effects

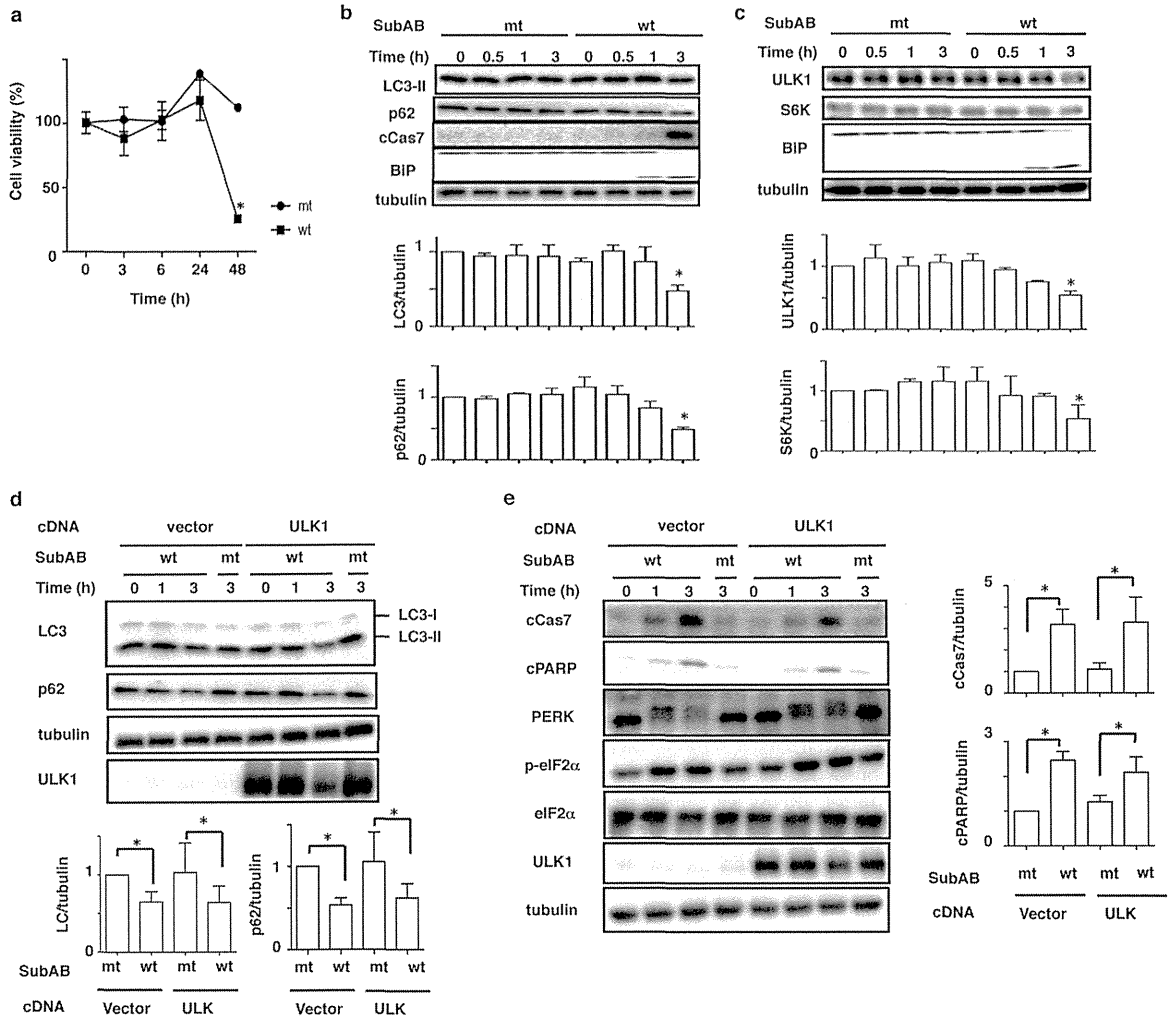

FIG 1 Effect of SubAB on autophagy in HeLa cells. (a) HeLa cells were incubated with catalytically inactivated (mt) or wild-type (wt) SubAB (200 ng/ml) for 0, 3, 6, 24, and 48 h. Cell viability with SubAB was determined with a Cell Counting kit as described in Materials and Methods. Data are means ± standard deviations of values from three experiments, with three duplicates per experiment ($n = 6$). *, $P < 0.05$. (b) HeLa cells were incubated with mt or wt SubAB (200 ng/ml) for 0, 0.5, 1, and 3 h. (Top) Cell lysates were analyzed by Western blotting using the indicated antibodies. (Bottom) The amounts of LC3-II and p62 after incubation with mt or wt SubAB were quantified by densitometry. Data are means ± standard deviations of values from three experiments. *, $P < 0.05$. (c) HeLa cells were treated with mt or wt SubAB for the indicated times. (Top) Cell lysates were analyzed by Western blotting using the indicated antibodies. (Bottom) The amounts of ULK1 and S6K after incubation with mt or wt SubAB were quantified by densitometry. Data are means ± standard deviations of values from three experiments. *, $P < 0.05$. (d) Cells transiently expressing Myc-tagged ULK1 were incubated with mt or wt SubAB for 3 h at 37°C. (Top) The amounts of LC3-II, p62, and ULK1 were determined by immunoblot analysis. (Bottom) The amounts of LC3-II and p62 after incubation with mt or wt SubAB for 3 h were quantified by densitometry. Data are means ± standard deviations of values from three experiments. *, $P < 0.05$. (e) Cells transiently expressing ULK1 cDNAs were treated with mt or wt SubAB for 0, 1, or 3 h at 37°C. (Left) Cell lysates were analyzed by Western blotting using specific antibodies as indicated. All experiments were repeated three times with similar results. (Right) The amounts of cCas7 and cPARP after incubation for 3 h with mt or wt SubAB were quantified by densitometry. Data are means ± standard deviations of values from three experiments. *, $P < 0.05$.

of SubAB on the mTOR-signaling pathway in PERK knockdown cells. In control siRNA-transfected cells, the amounts of phospho-mTOR, ULK1, phospho-ULK1, S6K, phospho-S6K, p62, and LC3-II were decreased by SubAB. In contrast, SubAB increased the levels of activation of caspase-7. In PERK knockdown cells, the expression level of PERK was significantly suppressed, and the amounts of ULK1, S6K, p62, and LC3-II were not decreased in the presence of SubAB. SubAB-induced caspase-7 activation was significantly suppressed in PERK knockdown cells, as described previously (12). The catalytically inactive SubAB had no effect (Fig. 2a).

We next investigated the effect of bafilomycin A1 (Baf A1) on the expression levels of LC3-II and p62 in the presence of SubAB in PERK knockdown cells. In control siRNA-transfected cells, the decreases in LC3-II and p62 levels by SubAB were not inhibited by Baf A1, which prevents the maturation of autophagic vacuoles (37). In PERK knockdown cells, the amounts of LC3-II and p62 were not decreased in the presence of mt or wt SubAB; they were, however, significantly increased in the presence of Baf A1 (Fig. 2b). As observed by confocal microscopy, SubAB decreased the number of cells showing LC3-II, even in the presence of Baf A1 (Fig. 2c, top). In contrast, in PERK knockdown cells, basal amounts of LC3-II were increased and were not significantly suppressed by SubAB with or without Baf A1 (Fig. 2c, bottom).

Previously, we demonstrated that SubAB-induced apoptosis is

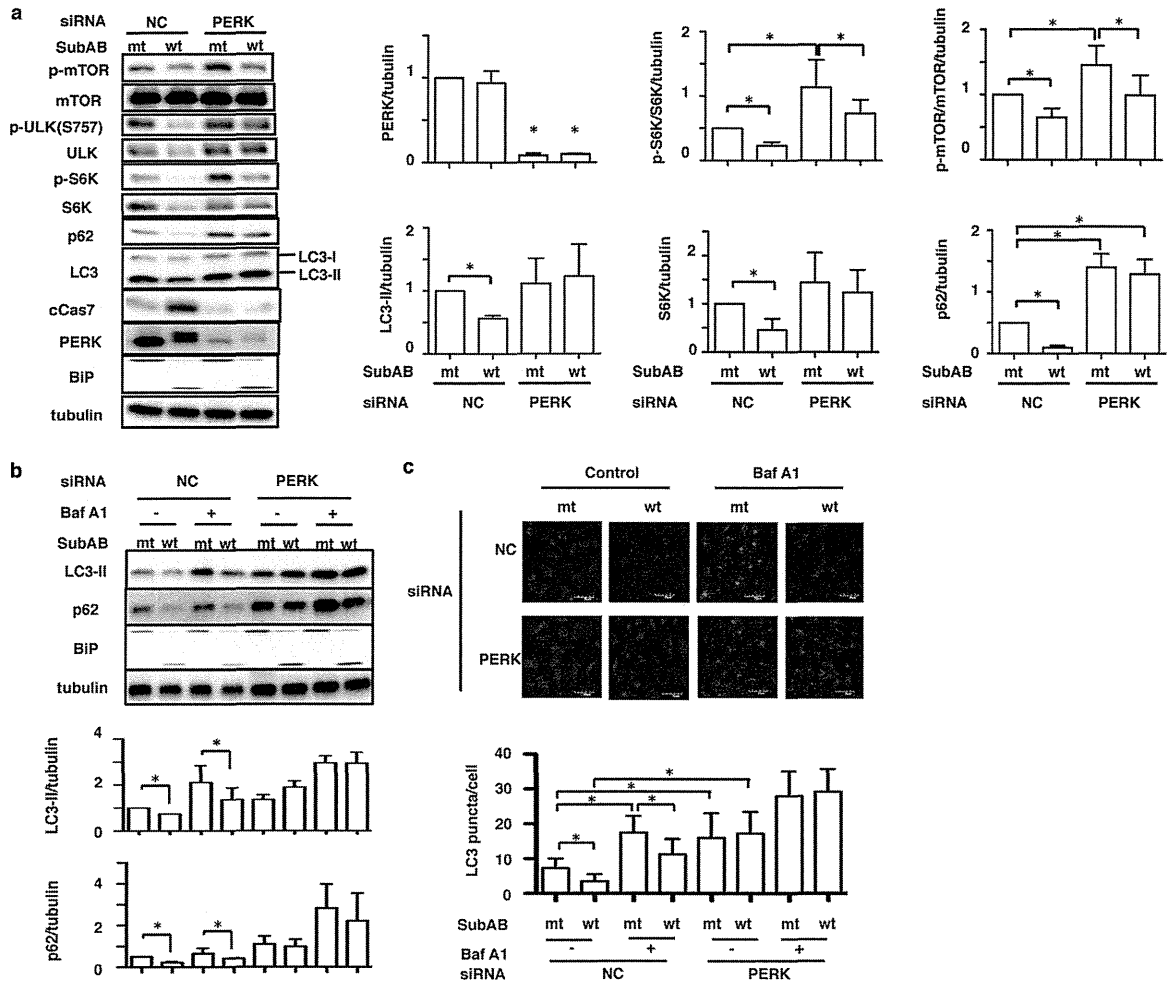

FIG 2 PERK controls apoptosis and autophagy by SubAB in HeLa cells. (a) Nontargeting control (NC) and PERK siRNA-transfected HeLa cells were incubated with mt or wt SubAB for 3 h. NC, nontargeting control siRNA. (Left) Cell lysates were analyzed by Western blotting using specific antibodies as indicated. (Right) The amounts of PERK, LC3-II, S6K, phospho-S6K (p-S6K), phospho-mTOR (p-mTOR), and p62 after incubation with mt or wt SubAB in control (NC) or PERK knockdown cells were quantified by densitometry. All experiments were repeated three times with similar results. Data are means ± standard deviations of values from three experiments. *, $P < 0.05$. (b) The siRNA-transfected HeLa cells were incubated with mt or wt SubAB in the presence or absence of 100 nM bafilomycin A1 (Baf A1) for 3 h. (Top) Cell lysates were analyzed by Western blotting using anti-LC3B, anti-p62, and anti-BiP antibodies. Tubulin was used as a loading control. (Bottom) The amounts of LC3-II and p62 were quantified by densitometry. All experiments were repeated three times with similar results. Data are means ± standard deviations of values from three experiments. *, $P < 0.05$. (c) (Top) The indicated siRNA-transfected HeLa cells were incubated with mt or wt SubAB in the presence or absence of 100 nM bafilomycin A1 (Baf A1) for 3 h, followed by fixation and then reaction with the indicated antibodies as described in Materials and Methods. (Bottom) The LC3 puncta in a single cell were manually counted under a confocal microscope (*, $P < 0.05$). For each group, 30 cells were randomly selected for averaging the number of LC3 puncta per cell.

caspase dependent (18). Recent studies have shown that apoptosis-mediated cleavage of Beclin 1 and Atg5 inhibits autophagy (38, 39). We next investigated the effect of SubAB on the expression of Atg5 and Beclin 1 in HeLa cells. SubAB treatment did not alter the amounts of Atg5 and Beclin 1 (Fig. 3a). We next examined if SubAB-induced caspase activation had an effect on the suppression of LC3-II and p62. A general caspase inhibitor, Z-VAD-FMK, completely suppressed SubAB-induced caspase-7 activation; however, SubAB action resulting in the reduction of LC3-II and p62 expression was not affected. Further, SubAB did not affect the amounts of Atg5 and Beclin 1. A necrosis inhibitor, Necrostatin, did not affect SubAB-induced reduction of LC3-II and p62 expression (Fig. 3b).

Furthermore, we investigated the effect of 3-methyladenine (3-MA), an autophagy inhibitor, on SubAB-suppressed LC3-II and p62. Although treatment with 3-MA enhanced SubAB-induced S6K dephosphorylation, 3-MA incubation did not alter SubAB-mediated BiP cleavage or SubAB-suppressed LC3-II and p62 expression (Fig. 3c, left). To examine whether autophagosome formation is involved in SubAB-induced apoptosis, we tested the effect of silencing of the Atg16L1 gene on SubAB-induced caspase activation. PERK knockdown dramatically suppressed SubAB-induced activation of caspase-7 and cleavage of PARP. The amounts of LC3-II and p62 were not decreased by SubAB in PERK knockdown cells (Fig. 2). Knockdown of Atg16L1 reduced the basal levels of LC3-II and Atg5 proteins. However, SubAB-induced PARP cleavage and caspase-7 activation were not affected by Atg16L1 knockdown. In PERK and Atg16L1 double-knockdown cells, SubAB-induced PARP cleavage and caspase-7 activation were not significantly increased over levels in mt

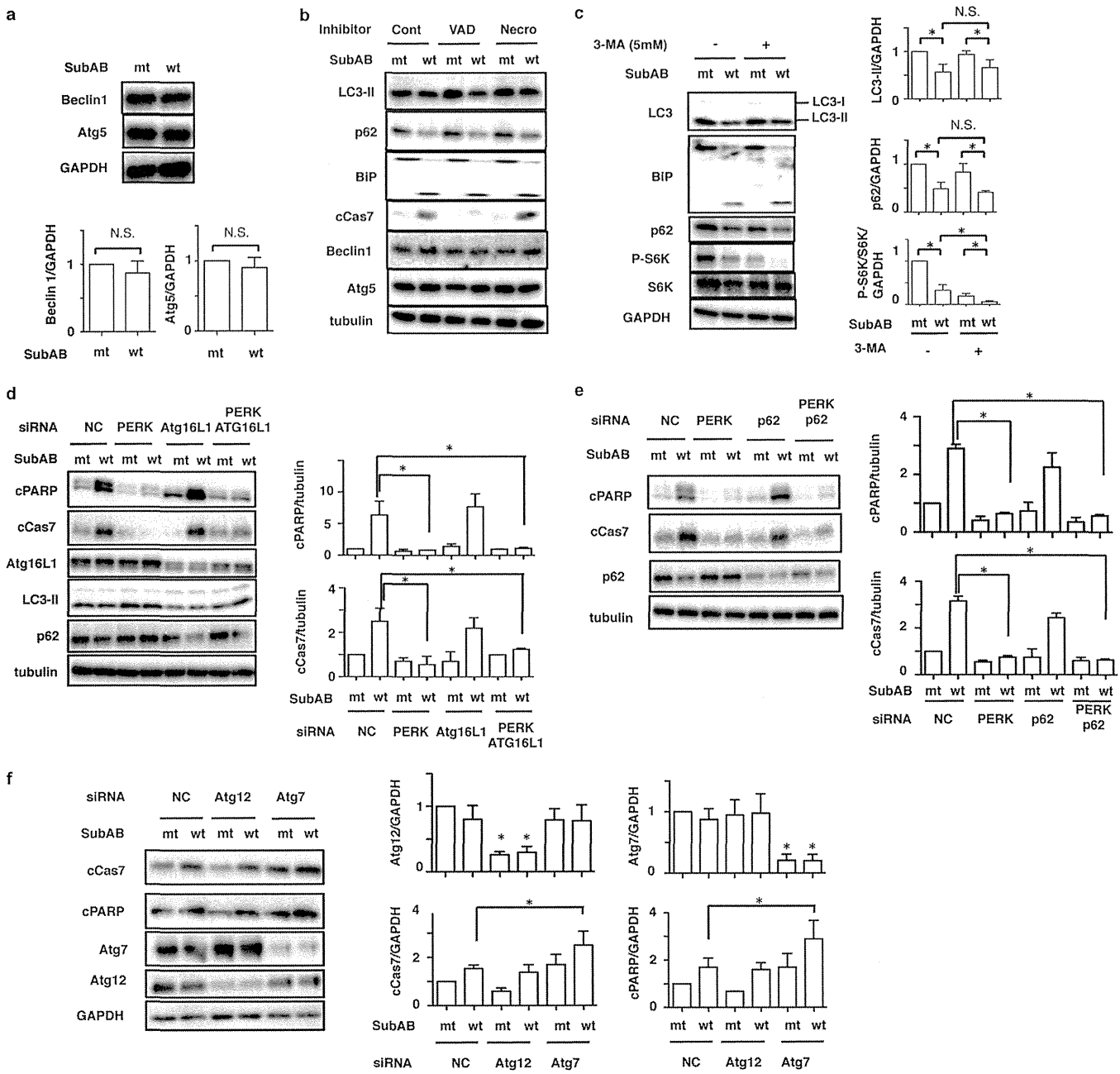

FIG 3 Effects of SubAB on autophagy-related proteins in HeLa cells. (a) HeLa cells were incubated with mt or wt SubAB for 3 h. Cell lysates were analyzed by Western blotting using anti-Beclin1 and anti-Atg5 antibodies. GAPDH was used as a loading control. N.S., not significant. (b) HeLa cells were pretreated with 10 μM Z-VAD-FMK (VAD) or 20 μM Necrostatin 1 (Necro) for 30 min and were then incubated with mt or wt SubAB for 3 h. Cell lysates were analyzed by Western blotting using specific antibodies as indicated. Cont, control. (c) HeLa cells were preincubated with 5 mM 3-methyladenine (3-MA) for 30 min and were then incubated with mt or wt SubAB for 3 h. (Left) Cell lysates were analyzed by Western blotting using specific antibodies as indicated. (Right) The amounts of LC3-II, p62, and p-S6K were quantified by densitometry. All experiments were repeated three times with similar results. Data are means ± standard deviations of values from three experiments. *, $P < 0.05$. (d and e) The indicated siRNA-transfected HeLa cells were incubated with mt or wt SubAB for 3 h. Cell lysates were analyzed by Western blotting using the indicated antibodies. The amounts of cPARP and cCas7 were quantified by densitometry. All experiments were repeated three times with similar results. Data are means ± standard deviations of values from three experiments. *, $P < 0.05$. (f) NC, Atg12, and Atg7 siRNA-transfected HeLa cells were incubated with mt or wt SubAB for 3 h. (Left) Cell lysates were analyzed by Western blotting using specific antibodies as indicated. All experiments were repeated three times with similar results. (Right) Atg7, Atg12, cCas7, and cPARP obtained with mt and wt SubAB were quantified by densitometry. Data are means ± standard deviations of values from three experiments. *, $P < 0.05$.

SubAB-treated cells (Fig. 3d). We next investigated the effects of p62 knockdown on SubAB-induced apoptosis. p62, a substrate of autophagy, is accumulated under autophagy-defective conditions and perturbs signal transduction pathways (36). As shown in Fig. 3e, p62 knockdown did not affect SubAB-induced PARP cleavage or caspase-7 activation. Taken together, these findings suggest that autophagosome-related proteins (e.g., Atg16L1, p62) do not affect SubAB-induced apoptosis. Further, we investigated

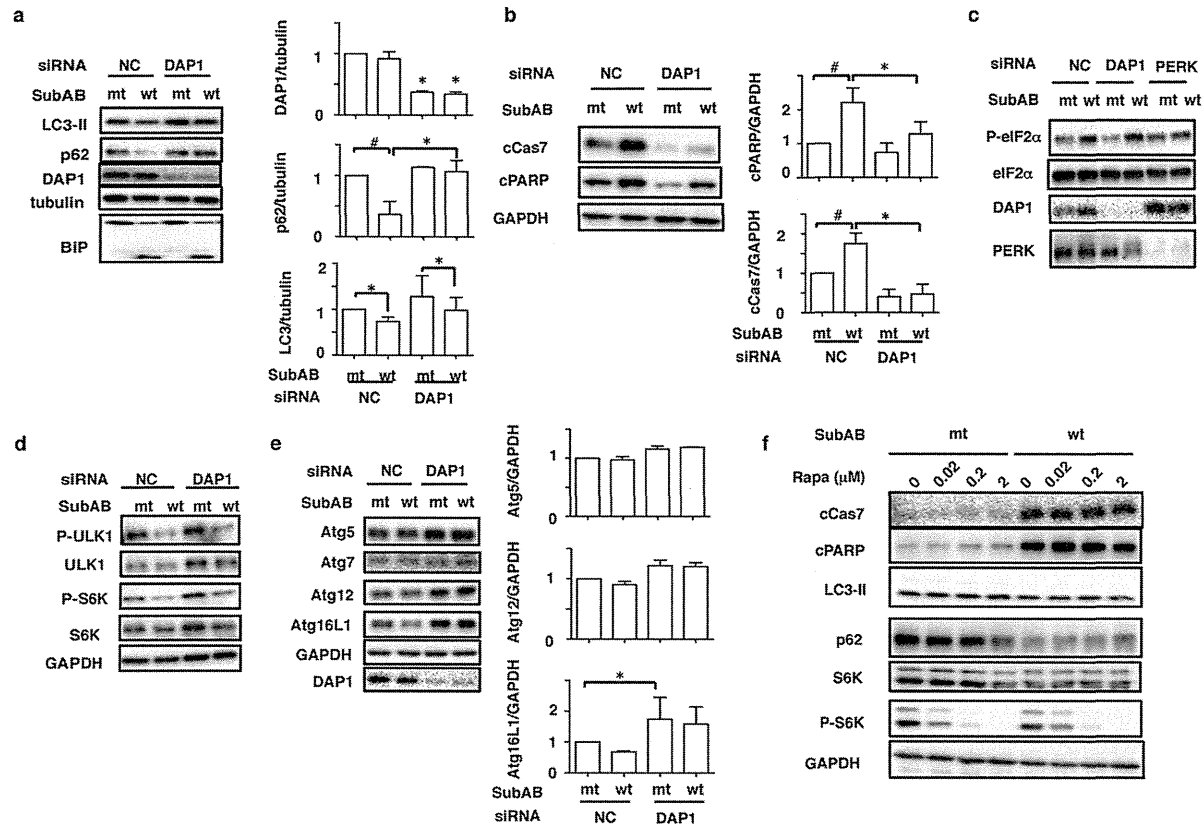

FIG 4 Knockdown of DAP1 rescues SubAB-mediated autophagy and apoptosis. (a) Nontargeting control (NC) and DAP1 siRNA-transfected HeLa cells (1×10^5/well) were incubated with mt or wt SubAB (0.2 μg/ml) for 3 to 4 h at 37°C. (Left) Cell lysates were analyzed by Western blotting using the indicated antibodies. (Right) The amounts of DAP1, p62, and LC3-II after incubation with mt or wt SubAB in NC or DAP1 knockdown cells were quantified by densitometry. All data are representative of the results of at least three separate experiments. Data are means ± standard deviations of values from three experiments. #, $P < 0.03$; *, $P < 0.05$. (b) NC and DAP1 siRNA-transfected cells were incubated with mt or wt SubAB (0.2 μg/ml) for 3 to 4 h at 37°C. (Left) Cell lysates were analyzed by Western blotting using anti-cCas7 and anti-cPARP antibodies. GAPDH was used as a loading control. (Right) The amounts of cCas7 and cPARP were quantified by densitometry. All data are representative of the results of at least three separate experiments. Data are means ± standard deviations of values from three experiments. #, $P < 0.03$; *, $P < 0.05$. (c) NC and DAP1 siRNA-transfected cells were incubated with wt or mt SubAB at 37°C for 2 h, followed by immunoblotting with anti-p-eIF2α(Ser51), anti-eIF2α, anti-DAP1, and anti-PERK antibodies. All data are representative of the results of at least three separate experiments. (d) NC and DAP1 siRNA-transfected cells were incubated with wt or mt SubAB at 37°C for 3 to 4 h, followed by immunoblotting with specific antibodies as indicated. (e) (Left) The siRNA-transfected cells were incubated and immunoblotted as described for panel d. (Right) The amounts of Atg5, Atg12, and Atg16L1 after incubation with mt or wt SubAB in NC or DAP1 knockdown cells were quantified by densitometry. All data are representative of the results of at least three separate experiments. Data are means ± standard deviations of values from three experiments. *, $P < 0.05$. (f) Cells were pretreated with the indicated concentrations of rapamycin (Rapa) for 1 h and were then incubated with mt or wt SubAB for 4 h, followed by immunoblotting with the indicated antibodies. All data are representative of the results of at least three separate experiments.

the effect of other types of Atg proteins, such as Atg12 and Atg7, on SubAB-induced apoptosis. Knockdown of Atg12, which is essential for autophagosome formation, did not affect SubAB-induced PARP cleavage or caspase activation. However, Atg7 knockdown significantly enhanced SubAB-induced apoptotic activity (Fig. 3f), as reported previously (40). These results suggest that Atg7 not only participates in autophagosome formation but also is involved in apoptosis.

Death-associated protein 1 (DAP1) plays an important role in SubAB-regulated apoptosis and autophagy. Since Atg family proteins were not associated with SubAB-regulated autophagy and apoptosis, as shown above, we next examined the role of DAP1, which has been reported to be an mTOR substrate and a negative regulator of autophagy (28, 41), in SubAB-regulated autophagy and apoptosis. First, we investigated the effect of siRNA-mediated knockdown of DAP1 on SubAB-associated apoptosis and autophagy. DAP1 expression was significantly suppressed by the siRNA. Depletion of DAP1 did not inhibit SubAB-mediated BiP cleavage. In control siRNA-transfected cells, SubAB treatment for 3 h significantly decreased LC3-II and p62 protein levels, while it increased caspase-7 activation and PARP cleavage. In contrast, in DAP1 knockdown cells, the basal level of DAP1 was decreased and SubAB treatment slightly decreased LC3-II and p62 levels, while SubAB-induced caspase-7 activation and PARP cleavage were significantly suppressed (Fig. 4a and b). To explore whether DAP1 regulates the PERK-eIF2α signaling pathway, we investigated, in DAP1 knockdown cells, the effect of SubAB on phospho-eIF2α. As shown in Fig. 4c, in control cells, SubAB increased eIF2α phosphorylation, which was not inhibited in DAP1 siRNA-transfected cells. As a positive control, in PERK knockdown cells, SubAB-induced eIF2α phosphorylation was suppressed. Thus, DAP1 acts downstream of SubAB-mediated BiP cleavage and PERK-eIF2α and controls both apoptosis and autophagy.

We next explored the effect of DAP1 depletion on mTOR sig-

naling by SubAB. A previous study showed that mTOR activity in HeLa cells was not affected by depletion of DAP1 (28). As shown in Fig. 4d, SubAB treatment significantly decreased phospho-ULK1 and phospho-S6K levels in DAP1 knockdown cells, effects similar to those seen in control siRNA-transfected cells, suggesting that these effects were independent of DAP1.

We also assessed the effect of DAP1 knockdown on the levels of Atg proteins. As shown in Fig. 4e, in control siRNA-transfected cells, SubAB treatment slightly decreased the amount of Atg16L1. Depletion of DAP1 increased the amounts of Atg5, Atg12, and Atg16L1, which were not decreased by SubAB.

Next, we investigated the effect of rapamycin, an mTOR complex 1 (mTORC1) inhibitor (42), on caspase activation by SubAB. It is known that rapamycin has protective effects against proapoptotic insults (40). S6K phosphorylation was suppressed by rapamycin in a dose-dependent manner. SubAB treatment decreased the amounts of LC3-II, p62, and S6K; rapamycin did not prevent caspase-7 activation or PARP cleavage by SubAB (Fig. 4f). Thus, rapamycin did not prevent the proapoptotic effects of SubAB.

DAP1 regulates Bax/Bak conformational changes, Bax/Bak oligomerization, and cytochrome *c* release. DAP1 affected SubAB-induced apoptosis and negatively regulated autophagy as shown above. Our previous studies and those of others showed that SubAB-induced apoptosis in HeLa cells was caused by Bax/Bak conformational changes and cytochrome *c* release, followed by caspase activation (12, 43, 44). We next examined the effect of the transfection of HeLa cells with DAP1 siRNA on SubAB-induced Bax/Bak conformational changes and Bax/Bak oligomerization by using conformation-specific anti-Bax (cBax) or anti-Bak (cBak) monoclonal antibodies. We also monitored the release of cytochrome *c* from mitochondria to the cytosol. Silencing of the DAP1 gene did not affect Bax and Bak levels. Densitometric analysis showed that SubAB-induced Bax/Bak conformational changes, Bax/Bak oligomerization, and cytochrome *c* (Cyt *c*) release were dramatically reduced in DAP1 knockdown cells from those in control siRNA-transfected cells (Fig. 5a and b).

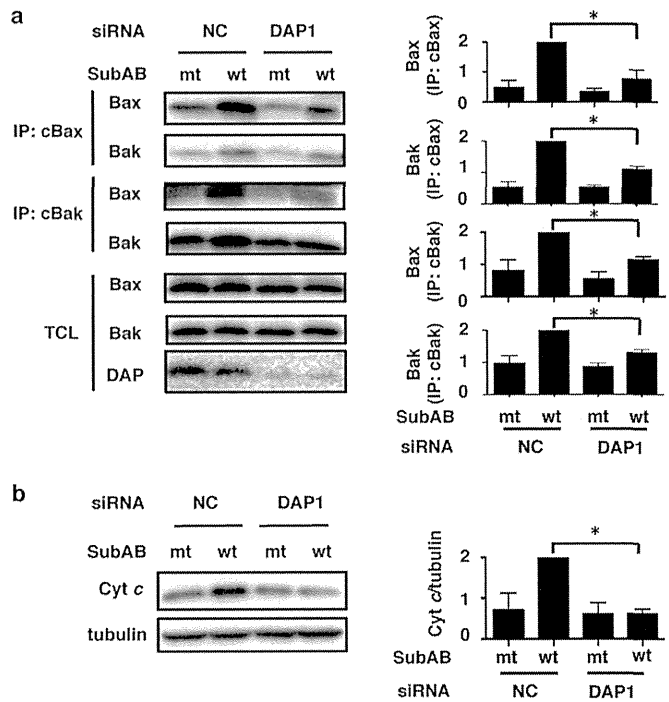

FIG 5 Depletion of DAP1 inhibits SubAB-induced Bak/Bax conformational changes. (a) NC and DAP1 siRNA-transfected cells were incubated with mt or wt SubAB (0.2 μg/ml) for 3 h at 37°C. Then cells were lysed, and proteins were immunoprecipitated with conformation-specific anti-Bax (cBax) or anti-Bak (cBak) monoclonal antibodies as described in Materials and Methods. The immunocomplexes (IP) or total-cell lysates (TCL) were analyzed by SDS-PAGE, followed by immunoblotting with anti-Bax and anti-Bak antibodies. (b) The level of cytochrome *c* (Cyt *c*) release into the cytoplasmic fraction was determined as described in Materials and Methods. Cytochrome *c* and tubulin were detected by Western blotting. Conformationally changed Bax, conformationally changed Bak, Bax/Bak complexes, and released Cyt *c* obtained with mt and wt SubAB were quantified by densitometry. Data are means ± standard deviations of values from three experiments. *, $P < 0.05$.

DISCUSSION

Recent studies have shown that several bacterial cytotoxins induced autophagy, which was associated with cell death (45–49). In contrast, cyclic AMP (cAMP)-elevating toxins from *Bacillus anthracis* and *Vibrio cholerae* suppressed host autophagy and thereby suppressed immune responses and modulated host cell physiology (50). It was also suggested that these toxins might disrupt a downstream step in autophagosome formation (50). Furthermore, it was demonstrated that cAMP-elevating toxins contribute to increased bacterial replication (50). In STEC infection, it is not known whether autophagy contributes to pathogenesis. SubAB was found mainly in non-O157, LEE-negative Stx2-producing STEC strains (51, 52). A recent study showed that Shiga toxins (Stxs), which are major virulence factors, induced autophagy in Stx-sensitive and Stx-insensitive cells (46). It showed that Stx-induced LC3-II generation depended on Stx B subunits, indicating that toxin enzymatic activity was not required for autophagosome formation; rather, toxin activity in sensitive cells was involved in caspase activation, leading to Atg5 and Beclin 1 cleavage (46). After treatment with SubAB, the amounts of Atg5 and Beclin 1 were unaltered. Pretreatment with a general caspase inhibitor (Z-VAD-FMK) or a necrosis inhibitor (Necrostatin) did not prevent SubAB-induced reduction of LC3-II and p62 levels, suggesting that SubAB-mediated inhibition of autophagy is not associated with inactivation or reduction of Atg proteins and Beclin 1 due to activation of caspase.

Here we show that SubAB toxin appears to suppress basal levels of autophagy in HeLa cells. Our results indicate that SubAB caused ER stress by BiP cleavage, resulting in the activation of a PERK-dependent pathway, leading to cell damage and a cytotoxic response, with suppression of autophagosome formation. This inhibition was not observed in PERK knockdown cells, where the basal level of LC3-II was significantly increased. Thus, a PERK-dependent pathway was involved in the SubAB-dependent decrease in autophagy.

Previous studies showed activation of PERK/eIF2α/ATF4 by the unfolded protein response, leading to inhibition of mTORC1–phospho-S6K signaling and the subsequent induction of cytoprotective autophagy (53, 54). We also investigated the effect of SubAB on mTORC1 signaling in HeLa cells. SubAB treatment decreased the levels of ULK1, S6K, phospho-ULK1, and phospho-S6K. Knockdown of PERK led to increases in the basal levels of ULK1 and S6K proteins, which were slightly reduced by SubAB treatment. In addition, we observed that SubAB decreased LC3-II and p62 protein levels even in ULK1-overexpressing cells. Thus, inhibition of autophagosome formation by SubAB is independent of ULK1-signaling pathways.

Several studies have identified factors responsible for the negative regulation of autophagy (55). We looked for candidate proteins that could serve as negative regulators of autophagy in SubAB-treated cells. Interestingly, we found that DAP1, which is expressed ubiquitously in many types of cells and tissues (28), is involved both in the suppression of autophagy by SubAB and in SubAB-induced apoptosis. DAP1 was identified as a novel substrate of mTOR that negatively regulates autophagy (28). Moreover, DAP1 has been shown to be a positive mediator of gamma interferon (IFN-γ)- and tumor necrosis factor alpha (TNF-α)-induced programmed cell death (30, 56). Silencing of the DAP1 gene in HeLa cells significantly inhibited the reduction in LC3-II and p62 expression seen with SubAB, effects similar to those of PERK knockdown. SubAB-induced phosphorylation of eIF2α was not altered by DAP1 depletion, suggesting that DAP1 was downstream of PERK-eIF2α. DAP1 knockdown did not affect the reduction of mTOR-dependent S6K phosphorylation by SubAB, suggesting that DAP1 may negatively regulate autophagy via an mTOR-independent pathway. Recent studies have shown that various factors, e.g., intracellular Ca^{2+}, cAMP, extracellular signal-regulated kinase (ERK), p38 mitogen-activated protein kinase (MAPK), reactive oxygen species (ROS), FoxO proteins, and transcription factor EB (TFEB), are involved in the induction of autophagy (57, 58). We did not observe any effect of an ERK inhibitor (U0126) on the protein levels of LC3-II and p62 or on the activation of caspase-7 by SubAB in DAP1 knockdown cells (data not shown). These results indicated that ERK phosphorylation did not participate either in the suppression of autophagy by SubAB or in SubAB-induced apoptosis through DAP1. We found that the levels of some proteins (e.g., ULK1, S6K) that were decreased by SubAB were significantly increased in DAP1 knockdown cells. The proteins whose levels were increased may be associated with mTOR-independent control of autophagy by DAP1 and may play an essential role in the reduction of autophagy by SubAB.

A previous report showed that DAP1 is functionally silenced in growing cells through mTOR-dependent phosphorylation of Ser3 and Ser51, with the dephosphorylated form of DAP1 acting as the active form that suppresses autophagy (28). To investigate whether the dephosphorylated form of DAP1 activates or inactivates the effects of SubAB, either FLAG-tagged DAP1, a nonphosphorylated (S3A S51A) mutant of DAP1, or the phosphomimetic (S3D S51D) mutant of DAP1 was transiently transfected into HeLa cells. However, these overexpressed DAP1 mutants did not alter SubAB-induced PARP cleavage from that with wild-type DAP1 (data not shown). Thus, our findings suggest that these DAP1 phosphorylation sites do not participate in SubAB-induced apoptosis. DAP1 may require other phosphorylation sites or an unknown interaction factor to participate in SubAB-induced apoptosis.

Further, we found that DAP1 was required for the stimulation of Bak/Bax-dependent apoptosis by SubAB. In SubAB-induced apoptosis, Bak/Bax conformational changes, Bak/Bax oligomerization, and cytochrome *c* release, leading to activation of caspases, were regulated by the ubiquitin-proteasome pathway (43, 44). Interestingly, sequence analysis of DAP1 showed that it is identical to promyelocytic leukemia (PML)-interacting clone 1 (PIC1) and sentrin, a Fas receptor-associated protein. These proteins share a significant degree of homology to ubiquitin and other ubiquitin homology proteins (56). In conclusion, we found that SubAB suppression of autophagy proceeded through a PERK-eIF2α-dependent pathway, which might promote STEC infection and participate in the pathogenesis of severe disease. Further, we showed here that DAP1 is a key regulator of both autophagy and apoptosis in cells intoxicated by SubAB. Recent studies have shown that DAP1 plays a proapoptotic role in human breast cancer (59). Loss of DAP1 in colorectal cancer cells resulted in a gain in cellular migration and a loss of sensitivity to apoptosis induced by a chemotherapeutic agent, 5-fluorouracil (5-FU) (60). Thus, DAP1 plays critical roles in cellular homeostasis and survival. Finally, understanding of DAP1-related signaling and its component proteins may help better characterize mTOR-independent autophagy and apoptosis.

ACKNOWLEDGMENTS

This work was supported by a Grant-in-Aid for Scientific Research from the Ministry of Education, Science and Culture of Japan and from the Improvement of Research Environment for Young Researchers program of the Japan Science and Technology Agency, as well as by grants-in-aid from the Ministry of Health, Labour, Welfare of Japan (H24-Shinkou-Ippan-012) and Takeda Science Foundation. Joel Moss was supported by the Intramural Research Program, National Institutes of Health, National Heart, Lung, and Blood Institute.

We acknowledge the expert technical assistance of K. Hirano.

REFERENCES

1. **Riley LW, Remis RS, Helgerson SD, McGee HB, Wells JG, Davis BR, Hebert RJ, Olcott ES, Johnson LM, Hargrett NT, Blake PA, Cohen ML.** 1983. Hemorrhagic colitis associated with a rare *Escherichia coli* serotype. N. Engl. J. Med. **308**:681–685. http://dx.doi.org/10.1056/NEJM198303243081203.
2. **Latorre-Martinez JC, Garcia-Lozano T, Blanco J, Buesa J.** 2007. Characterization of *Escherichia coli* O157:H7 strains isolated from sporadic cases of hemolytic-uremic syndrome in children. Enferm. Infecc. Microbiol. Clin. **25**:603–604. (In Spanish.) http://dx.doi.org/10.1157/13111190.
3. **Shiomi M, Togawa M.** 1997. Sporadic cases of hemolytic uremic syndrome and hemorrhagic colitis with serum IgM antibodies to lipopolysaccharides of enterohemorrhagic *Escherichia coli* O157. Nihon Rinsho **55**: 686–692. (In Japanese.)
4. **Karmali MA.** 2004. Prospects for preventing serious systemic toxemic complications of Shiga toxin-producing *Escherichia coli* infections using Shiga toxin receptor analogues. J. Infect. Dis. **189**:355–359. http://dx.doi.org/10.1086/381130.
5. **Paton AW, Srimanote P, Talbot UM, Wang H, Paton JC.** 2004. A new family of potent AB_5 cytotoxins produced by Shiga toxigenic *Escherichia coli*. J. Exp. Med. **200**:35–46. http://dx.doi.org/10.1084/jem.20040392.
6. **Cergole-Novella MC, Nishimura LS, Dos Santos LF, Irino K, Vaz TM, Bergamini AM, Guth BE.** 2007. Distribution of virulence profiles related to new toxins and putative adhesins in Shiga toxin-producing *Escherichia coli* isolated from diverse sources in Brazil. FEMS Microbiol. Lett. **274**: 329–334. http://dx.doi.org/10.1111/j.1574-6968.2007.00856.x.
7. **Tozzoli R, Caprioli A, Cappannella S, Michelacci V, Marziano ML, Morabito S.** 2010. Production of the subtilase AB_5 cytotoxin by Shiga toxin-negative *Escherichia coli*. J. Clin. Microbiol. **48**:178–183. http://dx.doi.org/10.1128/JCM.01648-09.
8. **Wu Y, Hinenoya A, Taguchi T, Nagita A, Shima K, Tsukamoto T, Sugimoto N, Asakura M, Yamasaki S.** 2010. Distribution of virulence genes related to adhesins and toxins in Shiga toxin-producing *Escherichia coli* strains isolated from healthy cattle and diarrheal patients in Japan. J. Vet. Med. Sci. **72**:589–597. http://dx.doi.org/10.1292/jvms.09-0557.
9. **Buvens G, Lauwers S, Pierard D.** 2010. Prevalence of subtilase cytotoxin in verocytotoxin-producing *Escherichia coli* isolated from humans and raw meats in Belgium. Eur. J. Clin. Microbiol. Infect. Dis. **29**:1395–1399. http://dx.doi.org/10.1007/s10096-010-1014-z.
10. **Byres E, Paton AW, Paton JC, Lofling JC, Smith DF, Wilce MC, Talbot UM, Chong DC, Yu H, Huang S, Chen X, Varki NM, Varki A, Rossjohn J, Beddoe T.** 2008. Incorporation of a non-human glycan mediates human susceptibility to a bacterial toxin. Nature **456**:648–652. http://dx.doi.org/10.1038/nature07428.

11. Yahiro K, Satoh M, Morinaga N, Tsutsuki H, Ogura K, Nagasawa S, Nomura F, Moss J, Noda M. 2011. Identification of subtilase cytotoxin (SubAB) receptors whose signaling, in association with SubAB-induced BiP cleavage, is responsible for apoptosis in HeLa cells. Infect. Immun. 79:617–627. http://dx.doi.org/10.1128/IAI.01020-10.
12. Yahiro K, Tsutsuki H, Ogura K, Nagasawa S, Moss J, Noda M. 2012. Regulation of subtilase cytotoxin-induced cell death by an RNA-dependent protein kinase-like endoplasmic reticulum kinase-dependent proteasome pathway in HeLa cells. Infect. Immun. 80:1803–1814. http://dx.doi.org/10.1128/IAI.06164-11.
13. Smith RD, Willett R, Kudlyk T, Pokrovskaya I, Paton AW, Paton JC, Lupashin VV. 2009. The COG complex, Rab6 and COPI define a novel Golgi retrograde trafficking pathway that is exploited by SubAB toxin. Traffic 10:1502–1517. http://dx.doi.org/10.1111/j.1600-0854.2009.00965.x.
14. Paton AW, Beddoe T, Thorpe CM, Whisstock JC, Wilce MC, Rossjohn J, Talbot UM, Paton JC. 2006. AB_5 subtilase cytotoxin inactivates the endoplasmic reticulum chaperone BiP. Nature 443:548–552. http://dx.doi.org/10.1038/nature05124.
15. Morinaga N, Yahiro K, Matsuura G, Moss J, Noda M. 2008. Subtilase cytotoxin, produced by Shiga-toxigenic *Escherichia coli*, transiently inhibits its protein synthesis of Vero cells via degradation of BiP and induces cell cycle arrest at G_1 by downregulation of cyclin D1. Cell. Microbiol. 10:921–929. http://dx.doi.org/10.1111/j.1462-5822.2007.01094.x.
16. Chong DC, Paton JC, Thorpe CM, Paton AW. 2008. Clathrin-dependent trafficking of subtilase cytotoxin, a novel AB_5 toxin that targets the endoplasmic reticulum chaperone BiP. Cell. Microbiol. 10:795–806. http://dx.doi.org/10.1111/j.1462-5822.2007.01085.x.
17. Morinaga N, Yahiro K, Matsuura G, Watanabe M, Nomura F, Moss J, Noda M. 2007. Two distinct cytotoxic activities of subtilase cytotoxin produced by Shiga-toxigenic *Escherichia coli*. Infect. Immun. 75:488–496. http://dx.doi.org/10.1128/IAI.01336-06.
18. Matsuura G, Morinaga N, Yahiro K, Komine R, Moss J, Yoshida H, Noda M. 2009. Novel subtilase cytotoxin produced by Shiga-toxigenic *Escherichia coli* induces apoptosis in Vero cells via mitochondrial membrane damage. Infect. Immun. 77:2919–2924. http://dx.doi.org/10.1128/IAI.01510-08.
19. Yamazaki H, Hiramatsu N, Hayakawa K, Tagawa Y, Okamura M, Ogata R, Huang T, Nakajima S, Yao J, Paton AW, Paton JC, Kitamura M. 2009. Activation of the Akt-NF-κB pathway by subtilase cytotoxin through the ATF6 branch of the unfolded protein response. J. Immunol. 183:1480–1487. http://dx.doi.org/10.4049/jimmunol.0900017.
20. Huang T, Wan Y, Zhu Y, Fang X, Hiramatsu N, Hayakawa K, Paton AW, Paton JC, Kitamura M, Yao J. 2009. Downregulation of gap junction expression and function by endoplasmic reticulum stress. J. Cell. Biochem. 107:973–983. http://dx.doi.org/10.1002/jcb.22202.
21. Tsutsuki H, Yahiro K, Suzuki K, Suto A, Ogura K, Nagasawa S, Ihara H, Shimizu T, Nakajima H, Moss J, Noda M. 2012. Subtilase cytotoxin enhances *Escherichia coli* survival in macrophages by suppression of nitric oxide production through the inhibition of NF-κB activation. Infect. Immun. 80:3939–3951. http://dx.doi.org/10.1128/IAI.00581-12.
22. Mizushima N, Yoshimori T, Ohsumi Y. 2011. The role of Atg proteins in autophagosome formation. Annu. Rev. Cell Dev. Biol. 27:107–132. http://dx.doi.org/10.1146/annurev-cellbio-092910-154005.
23. Yuk JM, Yoshimori T, Jo EK. 2012. Autophagy and bacterial infectious diseases. Exp. Mol. Med. 44:99–108. http://dx.doi.org/10.3858/emm.2012.44.2.032.
24. Patel KK, Stappenbeck TS. 2013. Autophagy and intestinal homeostasis. Annu. Rev. Physiol. 75:241–262. http://dx.doi.org/10.1146/annurev-physiol-030212-183658.
25. Rao VA, Klein SR, Bonar SJ, Zielonka J, Mizuno N, Dickey JS, Keller PW, Joseph J, Kalyanaraman B, Shacter E. 2010. The antioxidant transcription factor Nrf2 negatively regulates autophagy and growth arrest induced by the anticancer redox agent mitoquinone. J. Biol. Chem. 285:34447–34459. http://dx.doi.org/10.1074/jbc.M110.133579.
26. Kim HP, Wang X, Chen ZH, Lee SJ, Huang MH, Wang Y, Ryter SW, Choi AM. 2008. Autophagic proteins regulate cigarette smoke-induced apoptosis: protective role of heme oxygenase-1. Autophagy 4:887–895. http://dx.doi.org/10.4161/auto.6767.
27. Bolisetty S, Traylor AM, Kim J, Joseph R, Ricart K, Landar A, Agarwal A. 2010. Heme oxygenase-1 inhibits renal tubular macroautophagy in acute kidney injury. J. Am. Soc. Nephrol. 21:1702–1712. http://dx.doi.org/10.1681/ASN.2010030238.
28. Koren I, Reem E, Kimchi A. 2010. DAP1, a novel substrate of mTOR, negatively regulates autophagy. Curr. Biol. 20:1093–1098. http://dx.doi.org/10.1016/j.cub.2010.04.041.
29. Levy-Strumpf N, Kimchi A. 1998. Death associated proteins (DAPs): from gene identification to the analysis of their apoptotic and tumor suppressive functions. Oncogene 17:3331–3340.
30. Deiss LP, Feinstein E, Berissi H, Cohen O, Kimchi A. 1995. Identification of a novel serine/threonine kinase and a novel 15-kD protein as potential mediators of the gamma interferon-induced cell death. Genes Dev. 9:15–30. http://dx.doi.org/10.1101/gad.9.1.15.
31. Cooney R, Baker J, Brain O, Danis B, Pichulik T, Allan P, Ferguson DJ, Campbell BJ, Jewell D, Simmons A. 2010. NOD2 stimulation induces autophagy in dendritic cells influencing bacterial handling and antigen presentation. Nat. Med. 16:90–97. http://dx.doi.org/10.1038/nm.2069.
32. Pursiheimo JP, Rantanen K, Heikkinen PT, Johansen T, Jaakkola PM. 2009. Hypoxia-activated autophagy accelerates degradation of SQSTM1/p62. Oncogene 28:334–344. http://dx.doi.org/10.1038/onc.2008.392.
33. Jung CH, Jun CB, Ro SH, Kim YM, Otto NM, Cao J, Kundu M, Kim DH. 2009. ULK-Atg13-FIP200 complexes mediate mTOR signaling to the autophagy machinery. Mol. Biol. Cell 20:1992–2003. http://dx.doi.org/10.1091/mbc.E08-12-1249.
34. Mikhailov V, Mikhailova M, Degenhardt K, Venkatachalam MA, White E, Saikumar P. 2003. Association of Bax and Bak homo-oligomers in mitochondria. Bax requirement for Bak reorganization and cytochrome *c* release. J. Biol. Chem. 278:5367–5376. http://dx.doi.org/10.1074/jbc.M203392200.
35. Mizushima N, Yoshimori T. 2007. How to interpret LC3 immunoblotting. Autophagy 3:542–545. http://dx.doi.org/10.4161/auto.4600.
36. Pankiv S, Clausen TH, Lamark T, Brech A, Bruun JA, Outzen H, Overvatn A, Bjorkoy G, Johansen T. 2007. p62/SQSTM1 binds directly to Atg8/LC3 to facilitate degradation of ubiquitinated protein aggregates by autophagy. J. Biol. Chem. 282:24131–24145. http://dx.doi.org/10.1074/jbc.M702824200.
37. Klionsky DJ, Elazar Z, Seglen PO, Rubinsztein DC. 2008. Does bafilomycin A1 block the fusion of autophagosomes with lysosomes? Autophagy 4:849–950. http://dx.doi.org/10.4161/auto.6845.
38. Wirawan E, Vande Walle L, Kersse K, Cornelis S, Claerhout S, Vanoverberghe I, Roelandt R, De Rycke R, Verspurten J, Declercq W, Agostinis P, Vanden Berghe T, Lippens S, Vandenabeele P. 2010. Caspase-mediated cleavage of Beclin-1 inactivates Beclin-1-induced autophagy and enhances apoptosis by promoting the release of proapoptotic factors from mitochondria. Cell Death Dis. 1:e18. http://dx.doi.org/10.1038/cddis.2009.16.
39. Kang R, Zeh HJ, Lotze MT, Tang D. 2011. The Beclin 1 network regulates autophagy and apoptosis. Cell Death Differ. 18:571–580. http://dx.doi.org/10.1038/cdd.2010.191.
40. Ravikumar B, Berger Z, Vacher C, O'Kane CJ, Rubinsztein DC. 2006. Rapamycin pre-treatment protects against apoptosis. Hum. Mol. Genet. 15:1209–1216. http://dx.doi.org/10.1093/hmg/ddl036.
41. Koren I, Reem E, Kimchi A. 2010. Autophagy gets a brake: DAP1, a novel mTOR substrate, is activated to suppress the autophagic process. Autophagy 6:1179–1180. http://dx.doi.org/10.4161/auto.6.8.13338.
42. Sabers CJ, Martin MM, Brunn GJ, Williams JM, Dumont FJ, Wiederrecht G, Abraham RT. 1995. Isolation of a protein target of the FKBP12-rapamycin complex in mammalian cells. J. Biol. Chem. 270:815–822. http://dx.doi.org/10.1074/jbc.270.2.815.
43. May KL, Paton JC, Paton AW. 2010. *Escherichia coli* subtilase cytotoxin induces apoptosis regulated by host Bcl-2 family proteins Bax/Bak. Infect. Immun. 78:4691–4696. http://dx.doi.org/10.1128/IAI.00801-10.
44. Yahiro K, Morinaga N, Moss J, Noda M. 2010. Subtilase cytotoxin induces apoptosis in HeLa cells by mitochondrial permeabilization via activation of Bax/Bak, independent of C/EBP-homologue protein (CHOP), Ire1α or JNK signaling. Microb. Pathog. 49:153–163. http://dx.doi.org/10.1016/j.micpath.2010.05.007.
45. Liévin-Le Moal V, Comenge Y, Ruby V, Amsellem R, Nicolas V, Servin AL. 2011. Secreted autotransporter toxin (Sat) triggers autophagy in epithelial cells that relies on cell detachment. Cell. Microbiol. 13:992–1013. http://dx.doi.org/10.1111/j.1462-5822.2011.01595.x.
46. Lee MS, Cherla RP, Jenson MH, Leyva-Illades D, Martinez-Moczygemba M, Tesh VL. 2011. Shiga toxins induce autophagy leading to differential signalling pathways in toxin-sensitive and toxin-resistant human cells. Cell. Microbiol. 13:1479–1496. http://dx.doi.org/10.1111/j.1462-5822.2011.01634.x.
47. Gutierrez MG, Saka HA, Chinen I, Zoppino FC, Yoshimori T, Bocco JL, Colombo MI. 2007. Protective role of autophagy against *Vibrio cholerae*

cytolysin, a pore-forming toxin from *V. cholerae*. Proc. Natl. Acad. Sci. U. S. A. **104**:1829–1834. http://dx.doi.org/10.1073/pnas.0601437104.
48. **Di Venanzio G, Stepanenko TM, García Véscovi E.** 2014. *Serratia marcescens* ShlA pore-forming toxin is responsible for early induction of autophagy in host cells and is transcriptionally regulated by RcsB. Infect. Immun. **82**:3542–3554. http://dx.doi.org/10.1128/IAI.01682-14.
49. **Terebiznik MR, Raju D, Vazquez CL, Torbricki K, Kulkarni R, Blanke SR, Yoshimori T, Colombo MI, Jones NL.** 2009. Effect of *Helicobacter pylori*'s vacuolating cytotoxin on the autophagy pathway in gastric epithelial cells. Autophagy **5**:370–379. http://dx.doi.org/10.4161/auto.5.3.7663.
50. **Shahnazari S, Namolovan A, Mogridge J, Kim PK, Brumell JH.** 2011. Bacterial toxins can inhibit host cell autophagy through cAMP generation. Autophagy **7**:957–965. http://dx.doi.org/10.4161/auto.7.9.16435.
51. **Wolfson JJ, Jandhyala DM, Gorczyca LA, Qadeer Z, Manning SD, Hadler J, Rudrik JT, Thorpe CM.** 2009. Prevalence of the operon encoding subtilase cytotoxin in non-O157 Shiga toxin-producing *Escherichia coli* isolated from humans in the United States. J. Clin. Microbiol. **47**: 3058–3059. http://dx.doi.org/10.1128/JCM.00706-09.
52. **Paton AW, Paton JC.** 2005. Multiplex PCR for direct detection of Shiga toxigenic *Escherichia coli* strains producing the novel subtilase cytotoxin. J. Clin. Microbiol. **43**:2944–2947. http://dx.doi.org/10.1128/JCM.43.6.2944-2947.2005.
53. **Avivar-Valderas A, Bobrovnikova-Marjon E, Alan Diehl J, Bardeesy N, Debnath J, Aguirre-Ghiso JA.** 2013. Regulation of autophagy during ECM detachment is linked to a selective inhibition of mTORC1 by PERK. Oncogene **32**:4932–4940. http://dx.doi.org/10.1038/onc.2012.512.
54. **Hart LS, Cunningham JT, Datta T, Dey S, Tameire F, Lehman SL, Qiu B, Zhang H, Cerniglia G, Bi M, Li Y, Gao Y, Liu H, Li C, Maity A, Thomas-Tikhonenko A, Perl AE, Koong A, Fuchs SY, Diehl JA, Mills IG, Ruggero D, Koumenis C.** 2012. ER stress-mediated autophagy promotes Myc-dependent transformation and tumor growth. J. Clin. Invest. **122**:4621–4634. http://dx.doi.org/10.1172/JCI62973.
55. **Liang C.** 2010. Negative regulation of autophagy. Cell Death Differ. **17**: 1807–1815. http://dx.doi.org/10.1038/cdd.2010.115.
56. **Liou ML, Liou HC.** 1999. The ubiquitin-homology protein, DAP-1, associates with tumor necrosis factor receptor (p60) death domain and induces apoptosis. J. Biol. Chem. **274**:10145–10153. http://dx.doi.org/10.1074/jbc.274.15.10145.
57. **Lavallard VJ, Meijer AJ, Codogno P, Gual P.** 2012. Autophagy, signaling and obesity. Pharmacol. Res. **66**:513–525. http://dx.doi.org/10.1016/j.phrs.2012.09.003.
58. **Ravikumar B, Futter M, Jahreiss L, Korolchuk VI, Lichtenberg M, Luo S, Massey DC, Menzies FM, Narayanan U, Renna M, Jimenez-Sanchez M, Sarkar S, Underwood B, Winslow A, Rubinsztein DC.** 2009. Mammalian macroautophagy at a glance. J. Cell Sci. **122**:1707–1711. http://dx.doi.org/10.1242/jcs.031773.
59. **Wazir U, Jiang WG, Sharma AK, Mokbel K.** 2012. The mRNA expression of DAP1 in human breast cancer: correlation with clinicopathological parameters. Cancer Genomics Proteomics **9**:199–201.
60. **Jia Y, Ye L, Ji K, Toms AM, Davies ML, Ruge F, Ji J, Hargest R, Jiang WG.** 2014. Death associated protein 1 is correlated with the clinical outcome of patients with colorectal cancer and has a role in the regulation of cell death. Oncol. Rep. **31**:175–182. http://dx.doi.org/10.3892/or.2013.2866.

Cellular Microbiology (2014) **16**(10), 1582–1601

doi:10.1111/cmi.12315
First published online 17 June 2014

Uptake of Shiga-toxigenic *Escherichia coli* SubAB by HeLa cells requires an actin- and lipid raft-dependent pathway

Sayaka Nagasawa,[1] Kohei Ogura,[2] Hiroyasu Tsutsuki,[2] Hisako Saitoh,[1] Joel Moss,[3] Hirotaro Iwase,[1] Masatoshi Noda[2] and Kinnosuke Yahiro[2]*

[1]*Department of Legal Medicine, Graduate School of Medicine, Chiba University, Chiba 260-8670, Japan.*
[2]*Department of Molecular Infectiology, Graduate School of Medicine, Chiba University, Chiba 260-8670, Japan.*
[3]*Cardiovascular and Pulmonary Branch, National Heart, Lung, and Blood Institute, National Institutes of Health, Bethesda, MD 20892-1590, USA.*

Summary

The novel cytotoxic factor subtilase cytotoxin (SubAB) is produced mainly by non-O157 Shiga-toxigenic *Escherichia coli* (STEC). SubAB cleaves the molecular chaperone BiP/GRP78 in the endoplasmic reticulum (ER), leading to activation of RNA-dependent protein kinase (PKR)-like ER kinase (PERK), followed by caspase-dependent cell death. However, the SubAB uptake mechanism in HeLa cells is unknown. In this study, a variety of inhibitors and siRNAs were employed to characterize the SubAB uptake process. SubAB-induced BiP cleavage was inhibited by high concentrations of Dynasore, and methyl-β-cyclodextrin (mβCD) and Filipin III, but not suppressed in clathrin-, dynamin I/II-, caveolin1- and caveolin2-knockdown cells. We observed that SubAB treatment led to dramatic actin rearrangements, e.g. formation of plasma membrane blebs, with a significant increase in fluid uptake. Confocal microscopy analysis showed that SubAB uptake required actin cytoskeleton remodelling and lipid raft cholesterol. Furthermore, internalized SubAB in cells was found in the detergent-resistant domain (DRM) structure. Interestingly, IPA-3, an inhibitor of serine/threonine kinase p21-activated kinase (PAK1), an important protein of macropinocytosis, directly inhibited SubAB-mediated BiP cleavage and SubAB internalization. Thus, our findings suggest that SubAB uses lipid raft- and actin-dependent, but not clathrin-, caveolin- and dynamin-dependent pathways as its major endocytic translocation route.

Received 12 July, 2013; revised 7 May, 2014; accepted 8 May, 2014.
*For correspondence. E-mail yahirok@faculty.chiba-u.jp; Tel. (+81) 43 226 2048; Fax (+81) 43 226 2049.

Introduction

Subtilase cytotoxin (SubAB) is the prototype of a new AB_5 toxin family that was identified in Shiga toxigenic *Escherichia coli* (STEC) O113; H21 strain 98NK2, which was responsible for an outbreak of haemolytic uremic syndrome (HUS) (Paton *et al.*, 2004). After binding to the target cell receptor, SubAB is translocated into the cell, resulting in a site-specific cleavage of endoplasmic reticulum (ER) chaperone protein BiP/Grp78 (Paton *et al.*, 2006). Previous studies showed that BiP/Grp78 cleavage by SubAB triggers an ER stress response, leading to activation of various signalling and metabolic pathways, including transient inhibition of protein synthesis, cell cycle arrest in G_1 phase (Morinaga *et al.*, 2007) and RNA-dependent protein kinase (PKR)-like ER kinase (PERK) activation, followed by caspase-dependent apoptosis (Yahiro *et al.*, 2012). Recently, we demonstrated that SubAB-induced ER stress signals inhibited LPS-stimulated NO production through inhibition of NF-κB nuclear translocation and iNOS expression (Tsutsuki *et al.*, 2012).

Regarding SubAB entry, previous studies from our laboratory and elsewhere reported that SubAB first binds to N-linked terminal sialic acid-modified membrane proteins, such as α2β1 integrin (ITG) (Yahiro *et al.*, 2006; 2011) and N-glycolylneuraminic acid (Neu5Gc) -modified glycoproteins (Byres *et al.*, 2008). A recent paper reported that SubAB was internalized in Vero cells by clathrin-dependent endocytosis (Chong *et al.*, 2008). After being endocytosed, SubAB transport via Golgi involved a novel COG/Rab6/COPI-dependent pathway (Smith *et al.*, 2009).

Pathogen endocytosis is known to occur by pathways involving clathrin- and caveolae-mediated endocytosis, and macropinocytosis. Clathrin-mediated endocytosis, one of the best-studied receptor-dependent pathways, is

characterized by the formation of clathrin-coated pits, followed by their movement into the cytoplasm to form clathrin-coated vesicles. It plays an important role in neurotransmission, signal transduction and the regulation of many plasma membrane functions (McMahon and Boucrot, 2011).

Some small viruses (Sieczkarski and Whittaker, 2002) and Shiga-toxin produced by *E. coli* (Torgersen *et al.*, 2005) enter host cells using this pathway. The caveolae-mediated pathway is also involved in various cellular processes. Small vesicles termed caveolae, which are enriched in caveolin, cholesterol and sphingolipid (Hommelgaard *et al.*, 2005), have been implicated in the entry of the toxins (cholera and shiga toxin) (Nabi and Le, 2003), small viruses (e.g. SV40 virus; Hommelgaard *et al.*, 2005) and prions (Toni *et al.*, 2006).

Macropinocytosis is a pivotal endocytic route responsible for entry of pathogens into host cells (Sanchez *et al.*, 2012). It is an actin-dependent endocytic process, associated with vigorous plasma membrane activity in the form of ruffles or blebs (Mercer and Helenius, 2009), and regulated by kinases, such as phosphatidylinositol (PI) 3-kinase (PI3K) (Falcone *et al.*, 2006), Na^+/H^+ exchange (Sieczkarski and Whittaker, 2002; Sanchez *et al.*, 2013), intracellular Ca^{2+} (Jiang and Chen, 2009), protein kinase C, general kinases, DAG-lipase (Mercer and Helenius, 2008; Mercer *et al.*, 2010)and p21-activated kinase (PAK)1 (Dharmawardhane *et al.*, 2000).

Further, several recent studies demonstrated that clathrin-independent carriers/GPI-anchored protein-enriched endosomal compartment (CLIC/GEEC) pathway was also involved in viral infection (Nonnenmacher and Weber, 2011) and uptake of bacterial toxins (Harper *et al.*, 2013). A feature of endocytosis via the CLIC/GEEC is that it is functionally dependent on the actin cytoskeleton, membrane cholesterol, GRAF1, Cdc42 and Arf1, and that internalized vesicles are associated with a cholesterol-rich, detergent-resistant membrane (DRM)-containing GPI-anchored proteins and GRAF1 (Kumari *et al.*, 2010; Nonnenmacher and Weber, 2011).

We investigated SubAB uptake in HeLa cells, using pharmacological inhibitors, small interfering RNA (siRNA) gene silencing and confocal microscopy. We show that SubAB uptake is independent of dynamin, clathrin and caveolin pathway, and predominantly utilizes an actin and lipid raft-dependent pathway.

Results

SubAB entry is by a clathrin- and dynamin-independent pathway

A previous study reported that SubAB was endocytosed into Vero cells via a clathrin-dependent pathway (Chong *et al.*, 2008). However, it is not known whether this uptake pathway is specific to Vero cells and whether different pathways might be used in other cell types (e.g. HeLa cells).

Dynamin, a cytosolic GTPase, is required for clathrin-mediated endocytosis as well as for formation of caveolae but is not required for macropinocytosis (Henley *et al.*, 1998). To determine whether SubAB entry in HeLa cells requires dynamin, we first investigated the effect on SubAB uptake of Dynasore, a reversible inhibitor of dynamin1 and dynamin 2 GTPase activities, which is usually effective at 80 μM (Macia *et al.*, 2006). Cells were pretreated with the indicated concentrations of Dynasore for 30 min, and then incubated with SubAB for 1 h and its uptake and action were measured by quantifying BiP cleavage. The high concentration of Dynasore inhibited SubAB-induced BiP cleavage (Fig. 1A). In agreement, densitometric analysis also showed that Dynasore pretreatment resulted in a significant increase in the uncleaved form of 78 kDa BiP (Fig. 1B, left panel). To examine the role of clathrin-mediated endocytosis in SubAB action, we investigated the effect of two well-known clathrin inhibitors, chlorpromazine (CPZ) and monodansylcadaverine (MDC). It was reported that CPZ inhibits the assembly of coated pits at the plasma membrane (Eash *et al.*, 2004) and MDC specifically inhibits membrane-bound transglutaminase type 1 and thus interferes with protein–protein cross-linking reactions and hence clathrin-mediated vesicle formation (Kagan *et al.*, 2008). As shown in Fig. 1A and B (centre and right panels), pretreatment with the compounds inhibited SubAB-induced BiP cleavage. We next monitored SubAB internalization by using Alexa555-labelled SubAB in the presence or absence of 80 μM Dynasore. In control cells, SubAB bound to the cell surface, followed by internalization and accumulation in the ER, which contains BiP (Fig. S1A). SubAB entry was not inhibited by Dynasore (Fig. 1C) at this concentration; 200 μM Dynasore was also inactive (data not shown). The clathrin inhibitors, CPZ or MCD, did not inhibit SubAB uptake (Figs 1C and S1B). These data suggested that these inhibitors did not affect SubAB uptake, rather they obstructed movement to ER of SubAB after uptake.

To further explore the involvement of clathrin-mediated endocytosis on SubAB entry in HeLa cells, we tested the impact on SubAB uptake of siRNA-mediated downregulation of clathrin. As shown in Fig. 1D, clathrin expression was significantly suppressed by the siRNA. SubAB-mediated BiP cleavage was not inhibited in clathrin-knockdown cells. We used Alexa488-labelled transferrin as a positive control for clathrin-mediated transport. In control cells, both SubAB and transferrin were internalized and accumulated in the cytoplasm. In